Cyclovirobuxine D inhibits growth and progression of non-small cell lung cancer cells by suppressing the KIF11-CDC25C-CDK1-CyclinB1 G_2/M phase transition regulatory network and the NFκB/JNK signaling pathway

TING XUE[1], YAODONG CHEN[2], JIA XU[3], WEIQIN DU[4], PENGZHOU KONG[5] and XINRI ZHANG[1]

[1]State Key Laboratory for Pneumoconiosis of National Health Commission, Key Laboratory of Prevention, Treatment and Fundamental Studies for Respiratory Diseases of Shanxi, Department of Respiratory and Critical Care Medicine, First Hospital of Shanxi Medical University; [2]Department of Ultrasonic Imaging, First Hospital of Shanxi Medical University, Taiyuan, Shanxi 030001; [3]School of Medical Application Technology, Shenyang Medical College, Shenyang, Liaoning 110034; [4]Department of Clinical Laboratory, People's Hospital of Lüliang, Lüliang, Shanxi 033000; [5]Key Laboratory of Cellular Physiology of The Ministry of Education and Department of Pathology, Shanxi Medical University, Yingze, Taiyuan, Shanxi 030001, P.R. China

Received July 13, 2022; Accepted February 22, 2023

DOI: 10.3892/ijo.2023.5505

Abstract. Lung cancer is the leading cause of cancer-related mortality worldwide. Non-small cell lung cancer (NSCLC) is the most common pathological subtype of lung cancer and is associated with low 5-year overall survival rates. Therefore, novel and effective chemotherapeutic drugs are urgently required for improving the survival outcomes of patients with lung cancer. Cyclovirobuxine D (CVB-D) is a natural steroidal alkaloid, used for the treatment of cardiovascular diseases in Traditional Chinese Medicine. Several studies have also demonstrated the antitumor effects of CVB-D. Therefore, in the present study, the therapeutic effects of CVB-D in lung cancer and the underlying mechanisms were investigated using the *in vivo* xenograft model of NSCLC in nude mice and *in vitro* experiments with the NSCLC cell lines. Bioinformatics analyses of RNA-sequencing data, and cell-based functional assays demonstrated that CVB-D treatment significantly inhibited *in vitro* and *in vivo* NSCLC cell proliferation, survival, invasion, migration, angiogenesis, epithelial-to-mesenchymal transition and G_2/M phase cell cycle. CVB-D exerted its antitumor effects by inhibiting the KIF11-CDK1-CDC25C-cyclinB1 G_2/M phase transition regulatory oncogenic network and the NF-κB/JNK signaling pathway. CVB-D treatment significantly reduced the sizes and weights and malignancy of xenograft NSCLC tumors in the nude mice. In conclusion, the present study demonstrated that CVB-D inhibited the growth and progression of NSCLC cells by inhibiting the KIF11-CDK1-CDC25C-CyclinB1 G_2/M phase transition regulatory network and the NF-κB/JNK signaling pathway. Therefore, CVB-D is a promising drug for the treatment of NSCLC patients.

Correspondence to: Dr Pengzhou Kong, Key Laboratory of Cellular Physiology of The Ministry of Education and Department of Pathology, Shanxi Medical University, 56 South Xinjian Road, Yingze, Taiyuan, Shanxi 030001, P.R. China
E-mail: kongpengzhou@sxmu.edu.cn

Dr Xinri Zhang, State Key Laboratory for Pneumoconiosis of National Health Commission, Key Laboratory of Prevention, Treatment and Fundamental Studies for Respiratory Diseases of Shanxi, Department of Respiratory and Critical Care Medicine, First Hospital of Shanxi Medical University, 85 South Jiefang Road, Yingze, Taiyuan, Shanxi 030001, P.R. China
E-mail: ykdzxr61@163.com

Key words: cyclovirobuxine D, RNA-sequencing, non-small cell lung cancer, KIF11-CDC25C-CDK1-CyclinB1 signaling pathway, ultrasonic imaging

Introduction

Lung cancer is the leading cause of cancer incidence, morbidity and mortality worldwide (1). Non-small cell lung cancer (NSCLC) is the most common subtype of lung cancer that accounts for ~80% of lung cancer cases and is associated with low 5-year overall survival (OS) (2). Nearly 60% of patients with NSCLC are diagnosed with advanced or metastatic cancer (stages III and IV) and are not amenable for surgical treatment (3). Conventional radiotherapy and chemotherapy are the primary treatment strategies for NSCLC patients with advanced cancer. However, the 5-year OS rates of patients with advanced or metastatic NSCLC are low because of chemotherapy resistance, which is associated with driver gene mutations, epigenetic alterations and tumor heterogeneity (4). Therefore, there is an urgent need to develop novel chemotherapeutic drugs with fewer adverse effects to improve the survival outcomes in NSCLC.

Kinesin family member 11 (KIF11) is a mitotic kinesin belonging to the kinesin-like family of proteins. It is involved in the formation of the bipolar spindle and maintenance of prophase and prometaphase during mitosis (5). KIF11 plays a crucial role in cell division and is required for cell proliferation. KIF11 is overexpressed in several cancer types and is considered as a potential diagnostic and prognostic biomarker due to its significant association with neoplasia, tumor progression and poor survival outcomes (6-8). High KIF11 expression correlates with poor OS in NSCLC patients with lung adenocarcinoma (LUAD) (9,10). KIF11 is a promising diagnostic biomarker and therapeutic target in NSCLC (11,12). Therefore, targeted inhibition of KIF11 is a potential therapeutic strategy for NSCLC patients.

Natural plant compounds (NPCs) including resveratrol, curcumin and baicalin show antitumor properties including suppression of cancer cell proliferation and upregulation of cellular apoptosis, autophagy and cell cycle arrest (13-15). These anticancer NPCs inhibit epithelial-to-mesenchymal transition (EMT) by altering different cancer-related signal transduction pathways (16).

Cyclovirobuxine D (CVB-D, molecular formula: $C_{26}H_{46}N_2O$) is the main pharmaceutically active steroidal alkaloid that is isolated from the Chinese medicinal herb, *Buxus microphylla* (*B. microphylla*). CVB-D is widely used for the treatment of cardiovascular diseases as it demonstrates significant antioxidant, anti-inflammatory and autophagy-regulating properties (17). CVB-D also shows promising anticancer effects in hepatocellular carcinoma (HCC), colorectal cancer and glioblastoma multiforme cells (18-20). Zeng *et al* (21) showed that CVB-D-induced mitophagy and apoptosis in the lung cancer cells by activating the p65/BNIP3/LC3 signaling axis. However, the mechanisms by which CVB-D inhibits the growth and progression of lung cancer cells, particularly NSCLC cells are not well characterized. Therefore, in the present study, the therapeutic effects of CVB-D on the NSCLC cells and the underlying molecular mechanisms were investigated using the *in vivo* xenograft NSCLC model in nude mice and NSCLC cell lines.

Materials and methods

NSCLC cell lines, reagents and culture conditions. The NSCLC cell lines, A549 (cat no. SCSP-503) and H1299 (cat no. SCSP-589), and BEAS-2B (cat no. KCB200922YJ) were purchased from the Cell bank of the Chinese Academy of Sciences. The A549 and H1299 cells were cultured in RPMI-1640 medium (cat no. 01-100-1ACS; Biological Industries) containing 10% fetal bovine serum (FBS) (cat no. 04-001-1A; Biological Industries), 100 U/ml penicillin, and 100 mg/ml streptomycin. BEAS-2B cells were cultured in the serum-free medium for BEAS-2B cells purchased from the Cell bank of the Chinese Academy of Sciences (cat no. KCB M006). All the cell lines were cultured in a humidified chamber maintained at 37˚C and 5% CO_2. The stock solution of CVB-D (100 mmol/l; cat. no. C117989; Shanghai Aladdin Biochemical Technology Co., Ltd.) was prepared in methanol.

MTT assay. The cytotoxic effects of CVB-D on the NSCLC and BEAS-2B cells were analyzed using the MTT assay. The A549, H1299 and BEAS-2B cells ($5x10^3$ cells per well) were cultured for 24 h in 96-well plates, and treated with different concentrations of CVB-D (0-120 μM) for 24, 48 and 72 h. Then, 20 μl of 5 mg/ml MTT solution was added to each well and the plates were further incubated at 37˚C for 4 h. The formazan crystals were solubilized by adding 100 μl DMSO per well. The absorbance was recorded in a microplate reader at 490 nm. The assay was repeated thrice.

Colony formation assay. NSCLC cells ($1x10^3$/cells/well) were cultured in six-well plates for 24 h. Then, the cell culture medium was replaced with RPMI-1640 medium containing different doses of CVB-D (0-80 μM). The cells were further incubated at 37˚C for 24 h. Then, the culture supernatants were removed, and fresh culture medium (2 ml) was added to each well. The culture plates were incubated for 2 weeks to allow formation of visible colonies. The number of cells for a colony formation was >50 cells. The cells were then fixed with 4% paraformaldehyde (PFA) for 20 min and stained with 0.5% crystal violet at room temperature for 20 min. The colonies were counted manually and images were captured using a smartphone. The assay was repeated thrice.

Cell cycle assay. The A549 and H1299 cells ($2.5x10^5$ cells per well) were cultured in six-well plates for 24 h. Then, they were incubated with medium containing 40 μM CVB-D at 37˚C for a further 24 h. The cells were washed with phosphate-buffered saline (PBS) and fixed with 75% ethanol at 4˚C for 20 h. The fixed cells were washed twice with pre-chilled PBS and stained with Propidium iodide/RNaseA solution (cat no. MA0220; Dalian Meilun Biology Technology Co., Ltd.) at 4˚C for 30 min. Flow cytometry (FCM) was performed in a Novocyte flow cytometer (Agilent Technologies, Inc.) and the data was analyzed using the FlowJo VX software (FlowJo LLC) to determine the proportion of cells in multiple phases of the cell cycle.

Apoptosis assay. Cellular apoptosis was analyzed using the Annexin V-FITC/PI Apoptosis Detection Kit (cat no. MA0220; Dalian Meilun Biology Technology Co., Ltd.) according to the manufacturer's protocol. Briefly, the NSCLC cells were cultured overnight in six-well plates ($2.5x10^5$ cells per well) and treated with different doses of CVB-D (0-80 μM) at 37˚C for 24 h. Then, the cells ($1x10^6$ cells per sample) were washed with PBS, resuspended in Annexin V staining buffer, and stained with the Annexin V-FITC/PI cocktail in the dark at room temperature for 15 min. FCM was performed using the NovoCyte flow cytometer (Agilent Technologies, Inc.) and the data was analyzed using the FlowJo VX software to determine the proportion of apoptotic cells. The experiments were performed thrice.

Wound healing assay. NSCLC cells ($2.5x10^5$ cells/well) were cultured in six-well culture plates at 37˚C to generate a monolayer. The monolayers were wounded by scratching with a 200-μl micropipette tip. The cellular debris was removed by gently washing with PBS. The cells were then cultured in serum-free media containing different doses of CVB-D (0-20 μM) for 24 and 48 h. Then, the images of the monolayer were acquired and the migration of cells into the wounded

areas was analyzed using the ImageJ software (version 1.8.0; National Institutes of Health). The assay was repeated thrice times.

Transwell migration and Matrigel invasion assay. Transwell and Matrigel assays were used to analyze the migration and invasion, respectively, of NSCLC cells that were pre-treated with different concentrations of CVB-D (0-20 μM) for 48 h. Briefly, 200 μl serum-free medium containing untreated NSCLC cells ($5x10^4$ cells per well) or NSCLC cells pre-treated with 10 or 20 μM CVB-D ($7.5x10^4$ cells per well to compensate for cell death) was added in the upper chambers of the Transwell (cat no. 353097; BD) and 500 μl of RPMI-1640 medium supplemented with 10% FBS was added in the lower chambers of the 24-well plate. The polycarbonate membrane of the upper chamber was coated at 37˚C for 30 min with 100 μl of the Matrigel (cat no. BD356234; BD Biosciences) for the Matrigel invasion assay. The plates were incubated at 37˚C for 48 h in a humidified incubator. Then, the non-migratory or non-invasive cells were removed from the upper layer. The migratory or invasive cells were fixed with 4% PFA and stained with 0.5% crystal violet for 20 min. The stained cells were counted in three random visual fields under a light microscope (IX51; Olympus Corporation) and images were captured. The assay was performed thrice.

RNA-sequencing (RNA-seq) protocol. NSCLC cells ($2.5x10^5$ cells) were cultured overnight in six-cm culture dishes until they reached exponential growth. Then, they were cultured in RPMI-1640 medium with or without 50 μM CVB-D at 37˚C for 24 h. The cells were then digested with 1.0 ml RNAiso Plus reagent (Takara Biotechnology Co., Ltd.) and the cellular extract was stored at -80˚C. Total mRNA extraction and sequencing libraries were generated by the Shanghai Personal Biotechnology Co., Ltd. The concentration, quality and integrity of the mRNA samples was estimated using the NanoDrop 2000 spectrophotometer (Thermo Fisher Scientific, Inc.). The concentrations of mRNA samples were determined at 260 nm wavelength. The absorbance ratio of 260/280 nm (1.8-2.0) was used as an indicator of nucleic acid purity. Oligo dT-coupled magnetic beads were used to purify mRNAs with poly(A) tails from the total RNA samples. RNA fragmentation was performed using the NEBNext Ultra Directional RNA Library Prep Kit for Illumina (New England BioLabs, Inc.) with divalent cations in an Illumina proprietary fragmentation buffer at elevated temperature. The first strand cDNA was synthesized using random oligonucleotides and SuperScript II reverse transcriptase. The second strand was synthesized using DNA polymerase I and RNase H. The overhangs were converted into blunt ends using the exonuclease/polymerase activities. The aforementioned reagents including oligo dT-coupled magnetic beads, SuperScript II reverse transcriptase, DNA polymerase I, RNase H and exonuclease/polymerase were contained in the NEBNext Ultra II RNA Library Prep Kit for Illumina (cat no. E7530L; New England Biolabs, Inc.). Then, the 3'ends of the DNA fragments were adenylated and the Illumina PE adapter oligonucleotides were ligated. The cDNA fragments were purified using the AMPure XP system (Beckman Coulter, Inc.) and selectively enriched by PCR amplification. The PCR products were purified (AMPure XP system) and quantified using the Agilent high-sensitivity DNA assay in the Bioanalyzer 2100 system (Agilent 2100). The library was then sequenced using the NovaSeq 6000 platform (Illumina, Inc.) and a series of strict quality control steps were performed. The data from the final library was trimmed in comparison with the reference genome (Genome: Homo_sapiens.GRCh38.dna.primary_assembly.fa.; Database version: GRCh38.100; Genebuild by http://asia.ensembl.org/Homo_sapiens/Info/Index).

Bioinformatics analyses. The online DAVID 6.8 software (https://david.ncifcrf.gov/conversion.jsp) was used for gene identity (ID) conversion. Gene Expression Profiling Interactive Analysis (GEPIA)2 (http://gepia2.cancer-pku.cn) database was used to identify differentially expressed genes (DEGs) between the tumor and normal tissues, survival analysis and comparative analysis of the expression levels of multiple genes between datasets. The potential NSCLC therapeutic target genes were identified using the GeneCards database (https://www.genecards.org/). The Human Protein Atlas (HPA) database was used to estimate the KIF11 protein levels in the NSCLC LUAD tissues (http://www.proteinatlas.org). The potential CVB-D target genes were identified using the Swisstarget prediction database (http://www.swisstargetprediction.ch/index.php). All the DEGs from different datasets were imported into the Venny 2.1 online tool (https://bioinfogp.cnb.csic.es/tools/venny/index.html) to identify the overlapping genes. The String online database (https://cn.string-db.org/cgi/input?sessionId=buvVxyvCwXVT&input_page_show_search=on) was used to analyze the protein-protein association networks. The Gene Ontology (GO) and Kyoto Encyclopedia of Genes and Genomes (KEGG) pathway enrichment analyses of the downregulated DEGs was performed using the http://www.genome.jp/kegg and http://www.geneontology.org websites. The CVB-D targets were screened based on the following criteria: i) Oncogenes; ii) overexpressed in LUAD; iii) overexpressed oncogenes associated with lower OS; and iv) predicted CVB-D target genes.

Molecular docking. The canonical 3D structure of CVB-D (CAS No. 860-79-7) was obtained from PubChem (https://pubchem.ncbi.nlm.nih.gov/). The crystal structures of the KIF11, CDC25C and CDK1/cyclinB1 complex (PDB ID: 1X88, 3OP3 and 6GU2) were downloaded from the RCSB PDB database (http://www.rcsb.org/). AutoDock Tools (version 1.5.6) software was used to convert the PDB file format of CVB-D, KIF11, CDC25C, CDK1 and cyclinB1 to the PDBQT format and AutoDock Vina to perform the virtual molecular docking. Then, we selected the best docking pose was selected according to the score of binding energy. The docking image was acquired using Discovery Studio (version 2021).

Reverse transcription-quantitative polymerase chain reaction (RT-qPCR). Total RNA was extracted from NSCLC cells using the RNAiso Plus reagent (cat no. 9109) and reverse transcribed into cDNA using the Reverse transcription kit (cat no. RR047A; both from Takara Biotechnology Co., Ltd.) according to the manufacturer's instructions. Subsequently, cDNAs were amplified using the TB Green™ Premix Ex

Taq™ II (cat no. RR820A; Takara, Biotechnology Co., Ltd.) with the ABI Step One Plus Real-Time PCR system (Thermo Fisher Scientific, Inc.). The thermocycling conditions for qPCR amplification were as follows: Initial denaturation at 95˚C for 30 sec, followed by 40 cycles of 95˚C for 5 sec and 60˚C for 30 sec. The primer sequences used in the present study are listed in Table SI. The relative gene expression levels were estimated using the $2^{-\Delta\Delta Cq}$ method (22). GAPDH was used as the internal control. The experiment was repeated thrice.

Western blotting. NSCLC cells ($2.5x10^5$ cells/well) were incubated with CVB-D (0-80 μM) in six-well plates for 24 h. Then, after removing the medium, the cells were rinsed with pre-chilled PBS and lysed with RIPA lysis buffer (cat no. P0013B; Beyotime Institute of Biotechnology) containing protease and phosphatase inhibitors (cat nos. P6730 and P1260; Beijing Solarbio Science & Technology Co., Ltd.). The concentration of protein lysates was estimated using the BCA assay kit (cat. no. C503051; Sangon Biotech Co., Ltd.). Equal amounts (50 μg) of protein lysates were separated on 10% SDS-PAGE gels and then transferred onto PVDF membranes. The membranes were blocked with 5% BSA (cat no. A8020; Beijing Solarbio Science & Technology Co., Ltd.) at room temperature for 2 h containing buffer. Then, the membranes were incubated overnight at 4˚C with the following primary antibodies (diluted with 5% BSA): anti-proliferating cell nuclear antigen (PCNA; 1:2,000; cat no. 2586S), anti-Bax (1:1,000; cat no. 2772S), anti-Bcl-2 (1:1,000; cat no. 15071T), anti-Vimentin (1:1,000; cat no. 5741SS), anti-N-Cadherin (1:1,000; cat no. 4061S), anti-E-Cadherin (1:1,000; cat no. 3195S), anti-Slug (1:1,000; cat no. 9585S), anti-Snail (1:1,000; cat no. 3879S), anti-phosphorylated (p)-p65 (1:1,000; cat no. 3033S), anti-p65 (1:1,000; cat no. 8242S), anti-p-JNK (1:1,000; cat no. 9251S) and anti-JNK (1:1,000; cat no. 9252S); all from Cell Signaling Technology, Inc.; anti-CDK1 (1:500; cat no. AF6108), anti-CDC25c (1:500; cat no. AF6258), anti-CyclinB1 (1:500; cat no. AF6168) and anti-KIF11 (1:500; cat no. AF4745); all from Affinity Biosciences, Ltd.; and anti-GAPDH (1:1,000; cat no. abs830030; Absin Bioscience, Inc.). Then, the blots were incubated with one of the following secondary antibodies (diluted with 2% BSA): Goat anti-rabbit IgG-HRP (1:10,000; cat no. abs20040ss) and goat anti-mouse IgG-HRP (1:10,000; cat no. abs20039ss; both from from Absin Bioscience, Inc.). at room temperature for 1 h. The protein bands were developed using the electrochemiluminescence (ECL) reagent (cat no. 32106; Thermo Fisher Scientific, Inc. and detected using the Mini Chemiluminescent Imaging and Analysis System (MiniChemiTM 610; Beijing SageCreation Science & Technology Co., Ltd.; http://www.sinsitech.com/). The relative grayscale values of the protein bands were estimated using the ImageJ software. Western blotting experiments were repeated thrice.

Tumor xenograft experiments. A total of six female BALB/c nude mice (mean weight, 20±0.5 g; age, 5-6 weeks-old) were purchased from the Department of Experimental Animal Center, HFK Bioscience Co. Ltd (Beijing, China). The animal experiments were approved (approval no. 2021-114) by the Animal Ethics Committee of the First Hospital of Shanxi Medical University (Taiyuan, China). The mice were housed in a pathogen-free environment under controlled temperature (20-25˚C) and humidity (53-58%) with a 12/12-h light/dark cycle and provided with food and water *ad libitum*. Equal volumes (100 μl) of $1x10^7$ A549 cells resuspended in culture medium were injected subcutaneously into the flanks of the nude mice to establish tumor xenografts. After 7 days, the mice were randomly divided into the control and CVB-D intervention groups (n=3 per group). Physiological saline or CVB-D (20 mg/kg) were injected intraperitoneally into the control and CVB-D intervention group, respectively, once a day for 4 weeks. The xenograft tumor weights and volumes and the body weights of the xenograft tumor model mice in the control and CVB-D treatment groups were recorded during the process. In the process of the establishment of animal model in the present study, none of the mice succumbed. The mice were then sacrificed by CO_2 aspiration with 30% volume displacement rate per min, until the behavioral signs of pain or distress to inhaled CO_2 including jumps and paws at the nose and face, ataxia, labored breathing were disappeared (23). Histopathological analysis of the tumor tissues was performed to determine the effects of CVB-D on the growth and progression of the xenografted lung cancer cells.

Ultrasonic imaging (USI). USI (Philips Healthcare) was used to determine the *in vivo* therapeutic efficacy of CVB-D. The tumor growth was evaluated using the Bmode ultrasound. The degree of tumor hardness was estimated using ultrasonic elastosonography (USE). Tumor angiogenesis was evaluated using Color Doppler Flow Imaging (CDFI) and Color Power Angiography (CPA). Ultrasonic MicroPure Imaging (MI) was used to detect microcalcifications.

Histopathological examination. Hematoxylin and eosin (H&E) staining was performed to determine the histopathological changes in the xenograft tumors. The xenograft tumor model mice were euthanized on day 29 after CVB-D treatment. Tumor tissues were harvested, fixed at room temperature for >24 h with 4% PFA, embedded in paraffin, sectioned at 5-μm thick preparations with a microtome and stained with H&E at room temperature (hematoxylin for 5 min and eosin for 3-5 min). Images of the stained sections were captured using a light microscope.

Immunohistochemistry (IHC). IHC was performed using the UltraSensitive™ SP IHC kit (cat no. 9720; Fuzhou Maixin Biotech Co., Ltd.) according to the manufacturer's protocols. The paraffin-embedded xenograft tumor tissues were sectioned at 5-μm thick preparations, dewaxed with xylene (Tianjin Zhiyuan Chemical Reagents Co., Ltd.), and incubated for 20 min with sodium citrate buffer (pH 6.0) at 95˚C for antigen retrieval. Then, the slices were blocked for 30 min at 37˚C with goat serum (included in the UltraSensitive™ SP IHC kit) and incubated with primary antibodies (diluted with 5% BSA) overnight at 4˚C against the target proteins: anti-KIF11 (1:100; cat no. 23333-1-AP; from Proteintech Group, Inc.), anti-CDC25C (1:100; cat no. AF6258), anti-CDK1 (1:100; cat no. AF6108) and anti-cyclinB1 (1:100; cat no. AF6168; all from Affinity Biosciences, Ltd.); anti-Ki67 (1:100; cat no. A20018), anti-Bcl2 (1:100; cat no. A19693) and anti-N-Cadherin (1:100; cat no. A0433; all from ABclonal

Biotech Co., Ltd.). The slices were then incubated with the streptavidin-peroxidase complex at 37˚C for 30 min and color development was performed with the DAB detection kit (cat no. 0031; Fuzhou Maixin Biotech Co., Ltd.). The distribution, localization, and expression level of the target proteins were visualized and images were captured using a light microscope equipped with a digital camera. The integrated optical density was analyzed using the Image pro plus 6.0 software (Media Cybernetics, Inc.).

TUNEL assay. TUNEL Apoptosis Detection Kit (cat no. 11684817910; Roche Diagnostics) was used to determine the proportion of apoptotic cells in the xenograft tumor tissues. The dewaxed sections of the tumor tissues were processed according to the manufacturer's protocol. Images of six randomly selected visual fields were captured per slide using a light microscope and the proportions of apoptotic cells were estimated.

Transient transfection of small interfering (si)RNA. A549 and H1299 cells were transfected for 48 h with the negative control siRNA (si-NC), or siRNAs against KIF-11 (si-KIF11; cat no. SIGS0001287-4) or cyclinB1 (si-CyclinB1; cat no. SIGS0003277-4) using the RiboFECT CP Transfection Kit (C10511-05; all from Guangzhou RiboBio Co., Ltd.) according to the manufacturer's instructions. The concentration of siRNAs used in the present study was 50 nM. Subsequent experiments were performed after transfection for 48 h at 37˚C. The control, KIF11-silenced cells and cyclinB1-silenced cells were used for subsequent experiments. The transfection controls used for each siRNA experiment were contained in the corresponding commercial kits. The sequences for si-KIF11 and si-cyclinB1 are listed in Table SII. The sequence for si-NC was not disclosed because the RiboBio Co., Ltd. applied for patent protections for their commercial siRNA kits.

Statistical analysis. Statistical analysis was performed using the SPSS 13.0 statistical software (SPSS, Inc.). All data are presented as the mean ± standard deviation and the results were presented using the GraphPad Prism version 7.0 software (GraphPad software Inc.). The differences in data between two groups were analyzed using the paired Student's t-test after testing for normality and homogeneity of variance. The differences in data between multiple groups were analyzed using the one-way analysis of variance (ANOVA) and the Bonferroni method as post hoc. Correlation among the DEGs was evaluated using Pearson's correlation analysis. $P<0.05$ was considered to indicate a statistically significant difference.

Results

CVB-D inhibits in vitro proliferation of NSCLC cells by inducing cell cycle arrest in the G_2/M phase. MTT assay results showed that CVB-D treatment significantly reduced the viability of A549 and H1299 cells in a dose- and time-dependent manner (Fig. 1A). The 50% inhibitory concentration (IC_{50}) values of CVB-D for the A549 and H1299 cells based on the Probit regression analysis were 68.73 and 61.16 μM at 24 h, 59.46 and 54.99 μM at 48 h, and 47.78 and 41.7 μM at 72 h, respectively. Furthermore, at the concentrations used in this assay, CVB-D treatment did not induce cytotoxicity in the BEAS-2B cells (Fig. S1). This data demonstrated the therapeutic potential of CVB-D to treat resistant lung cancer. CVB-D treatment significantly reduced the colony formation ability of the NSCLC cells in a dose-dependent manner (Fig. 1B and C). Furthermore, CVB-D treatment induced G_2/M cell cycle arrest of the NSCLC cells (Fig. 1D-F). The percentages of CVB-D-treated A549 and H1299 cells in the G_2/M phase were significantly higher than those in the control groups (Fig. 1E and F). CyclinB1 is a checkpoint protein that regulates G_2/M phase progression of the cell cycle (24). Western blot results demonstrated that CVB-D treatment significantly decreased expression levels of the cyclinB1 protein in the NSCLC cells (Fig. S2A and B). These results suggested that CVB-D inhibited proliferation of NSCLC cells by inducing cell cycle arrest in the G_2/M phase.

CVB-D treatment induces apoptosis of NSCLC cells. It was then analyzed whether CVB-D promoted apoptosis of the NSCLC cells. FACS analysis revealed that CVB-D treatment induced apoptosis of A549 and H1299 cells in a concentration-dependent manner (Fig. 2A and B). Furthermore, western blot analysis showed that CVB-D treatment significantly decreased Bcl-2 protein levels and increased Bax protein levels in the NSCLC cells (Fig. 2C and D). This demonstrated that CVB-D treatment induced *in vitro* apoptosis of the NSCLC cells.

CVB-D inhibits migration and invasion of NSCLC cells in a dose-dependent manner. Next, the effects of CVB-D on the migration and invasiveness of the NSCLC cells were analyzed. The A549 and H1299 cells were treated with sub-lethal concentrations of CVB-D (0-20 μM) in the wound healing assays to eliminate cell viability effects. Wound healing assay results showed that CVB-D treatment significantly decreased the wound healing rate or the migration rate of the NSCLC cells in a concentration-dependent manner (Fig. 3A and B). Furthermore, Transwell assays demonstrated that CVB-D treatment significantly decreased the number of migratory and invasive NSCLC cells in a concentration-dependent manner (Fig. 3C and D). Overall, these results demonstrated that treatment with sub-lethal concentrations of CVB-D inhibited the migration and invasion of NSCLC cells in a dose-dependent manner.

CVB-D treatment inhibits EMT, invasion and migration of NSCLC cells. Western blot assays were then performed to determine the levels of EMT-related biomarkers including E-cadherin, vimentin and N-cadherin in the CVB-D treated NSCLC cells. CVB-D treatment significantly increased the expression levels of E-cadherin and decreased the expression levels of N-cadherin and vimentin (Fig. 4A and B). This demonstrated that CVB-D inhibited EMT in the NSCLC cells. PCNA is a known proliferation biomarker due to its critical role in DNA metabolism and synthesis, replication and repair (25). Furthermore, Snail and Slug are essential transcriptional factors that promote cell migration during tumorigenesis and metastasis in multiple cancers (26). Western blot analysis demonstrated that CVB-D treatment significantly decreased

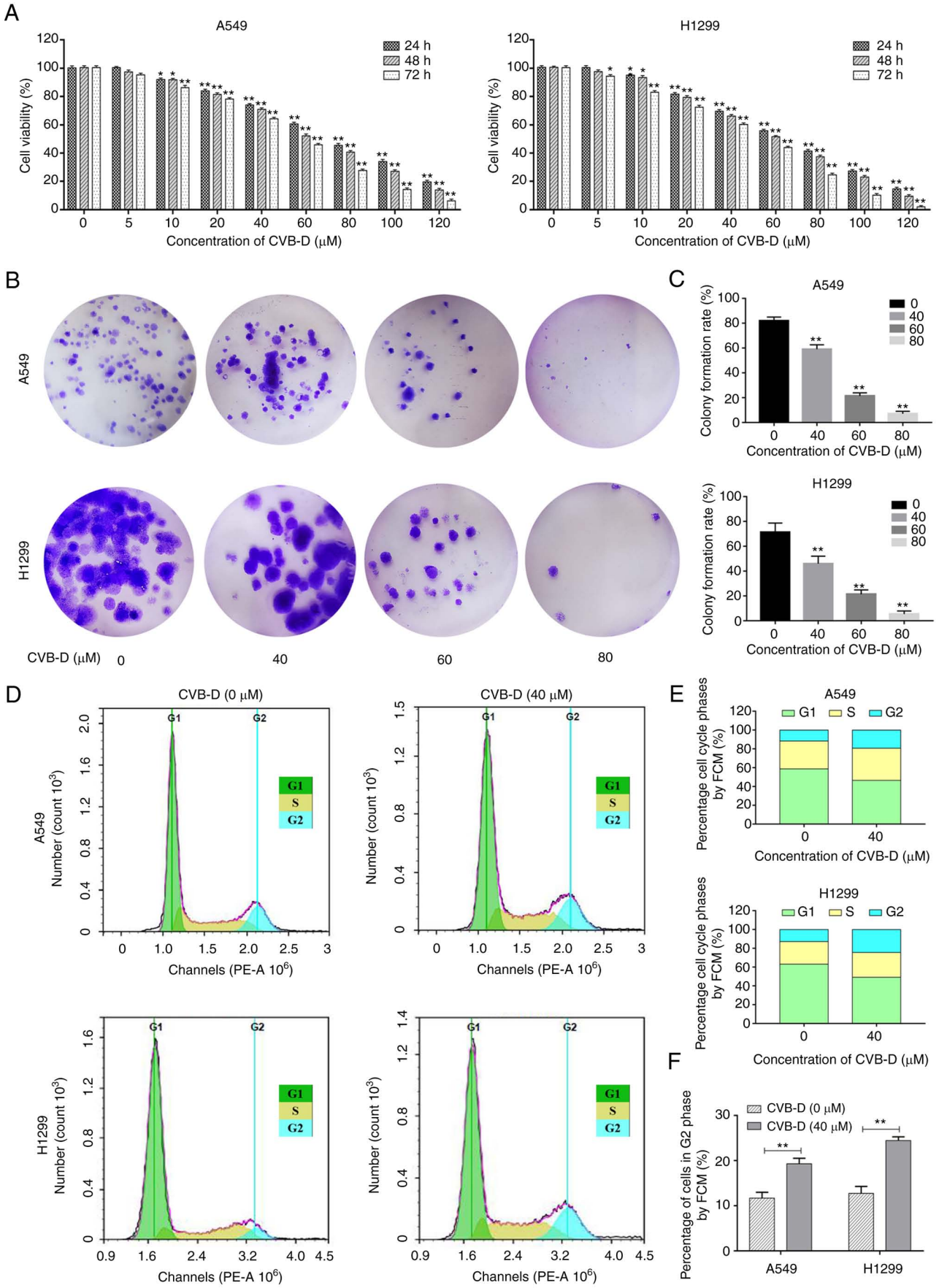

Figure 1. CVB-D inhibits proliferation of NSCLC cells in a dose-dependent manner. (A) MTT assay results revealed the viability of NSCLC cells treated with various concentrations of CVB-D (0-120 μM) at 24, 48 and 72 h. (B and C) Colony-formation assay results showed the effects of different concentrations of CVB-D (0-80 μM) on the colony-formation ability assay of NSCLC cells. (D and E) FCM results demonstrated the effects of CVB-D treatment on the cell cycle progression of NSCLC cells. (F) The percentage of G_2 phase NSCLC after treatment with CVB-D as analyzed by FCM. *P<0.05 and **P<0.01 vs. control group. CVB-D, cyclovirobuxine D; NSCLC, non-small cell lung cancer; FCM, flow cytometry.

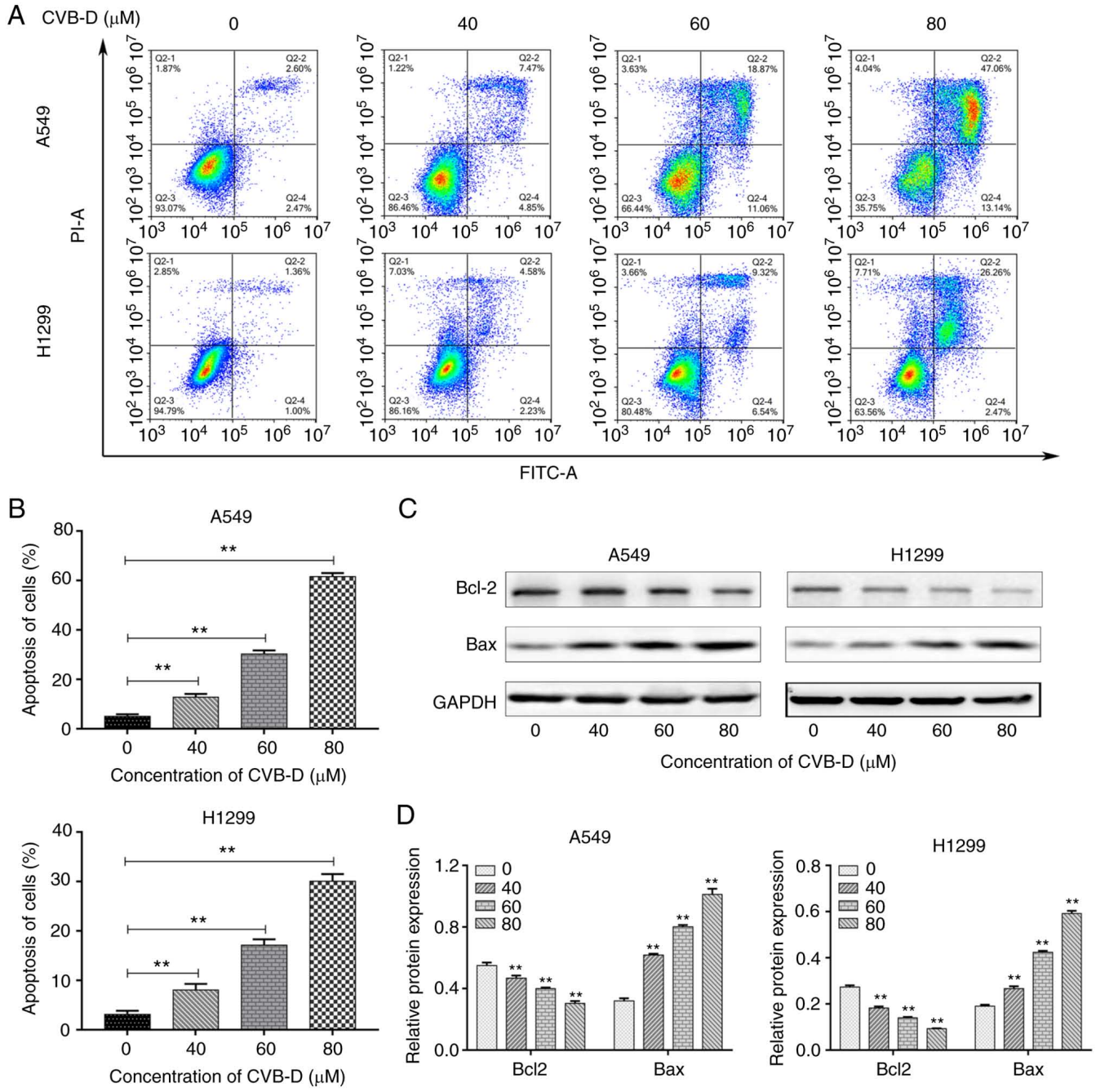

Figure 2. CVB-D promotes apoptosis of NSCLC cells. (A) Flow cytometric assay results showed the percentage of apoptotic cells in the NSCLC cell cultures treated with different concentrations of CVB-D (0-80 μM). The cells were stained by Annexin V-FITC and PI. (B) The histogram plots revealed the percentage of apoptotic NSCLC cells treated with different concentrations of CVB-D. (C and D) Western blot assay results demonstrated the expression levels of Bcl-2 and Bax proteins in the NSCLC cells treated with different concentrations of CVB-D. **P<0.01 vs. control (0 mM of CVB-D). CVB-D, cyclovirobuxine D; NSCLC, non-small cell lung cancer; FITC, fluorescein isothiocyanate; PI, propidium iodide.

the expression levels of PCNA, Snail and Slug proteins in the NSCLC cells in a dose-dependent manner (Fig. 4A and B). These results demonstrated that CVB-D inhibited proliferation, G_2/M phase cell cycling, survival, migration and invasion of the NSCLC cells.

CVB-D treatment inhibits NF-κB/JNK signaling pathway in the NSCLC cells. Next, RNA-seq analysis was performed to identify the molecular mechanisms underlying the effects of CVB-D treatment on the NSCLC cells (Fig. 5A). Before performing the differential expression analysis, Pearson's correlation analysis was performed between the control and CVB-D-treated samples. Pearson's correlation coefficients were close to 1, thereby indicating high correlation in the expression patterns between the samples (Fig. 5B). Principal component analysis demonstrated satisfactory repeatability in the treatment and the selection of samples (Fig. 5C). The heatmap revealed clustering of DEGs between the control and CVB-D treatment groups (Fig. 5D). Bidirectional cluster analysis was performed to identify DEGs between the CVB-D-treated NSCLC cells and the control untreated NSCLC cells. Volcano plots showed 4244 DEGs including

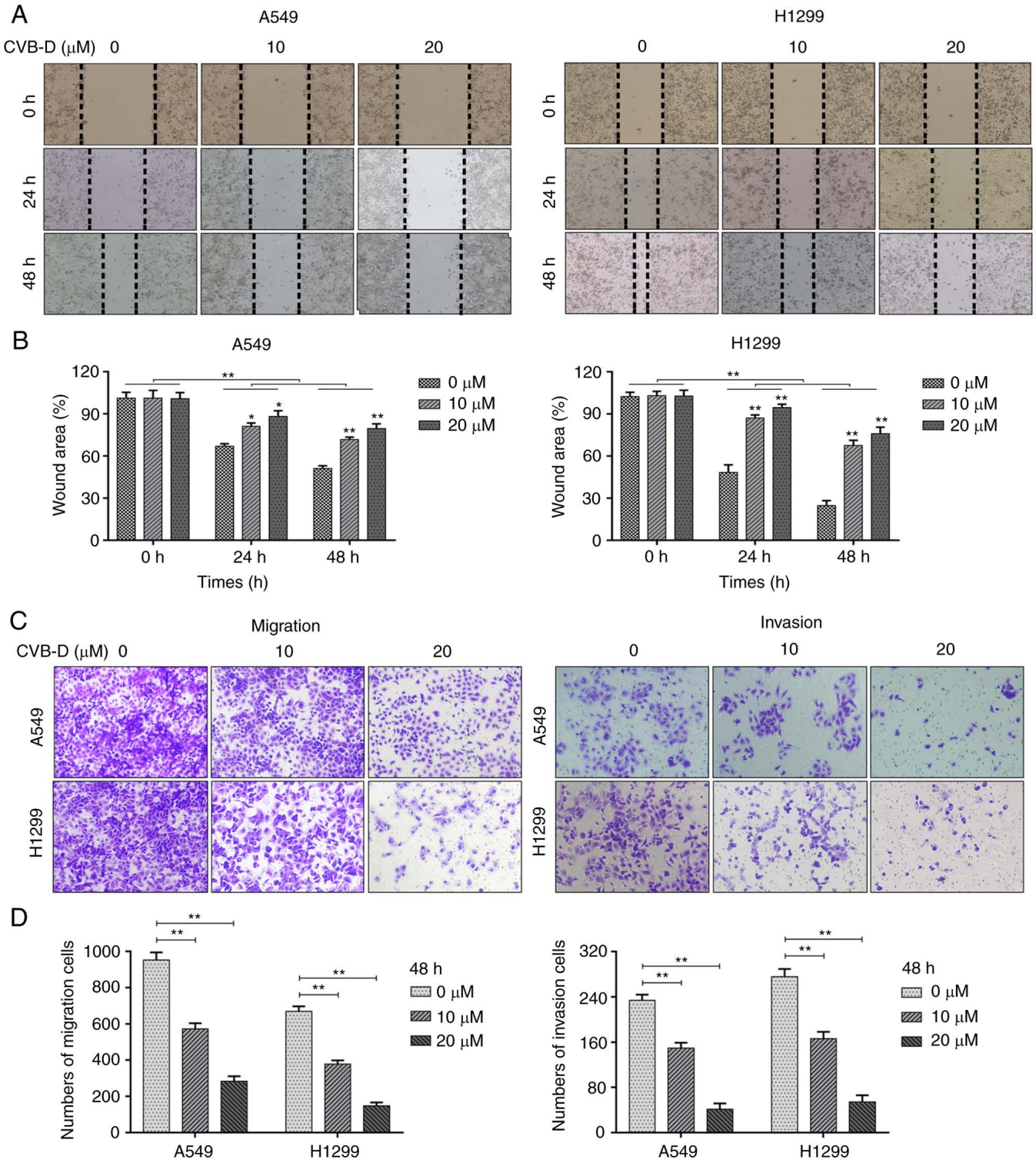

Figure 3. CVB-D treatment inhibits migration and invasiveness of NSCLC cells. (A and B) Wound healing assay results revealed the migration status of NSCLC cells after treatment with sub-lethal concentrations of CVB-D (0-20 μM). (C and D) Transwell migration and invasion assay results showed the numbers of migrating and invasive NSCLC cells after treatment with sub-lethal concentrations of CVB-D (0-20 μM). *P<0.01 and **P<0.01 vs. control (0 mM of CVB-D). CVB-D, cyclovirobuxine D; NSCLC, non-small cell lung cancer.

2115 upregulated DEGs and 2129 downregulated DEGs in the CVB-D-treated NSCLC cells (Fig. 5E and F). Functional enrichment analysis of the downregulated DEGs demonstrated enrichment of GO terms related to molecular functions (MF) including 'DNA binding' and 'ion binding', GO terms related to cellular components (CC) including 'intracellular' and 'intracellular part' and GO terms related to biological processes (BP) including 'RNA biosynthetic process' and 'heterocycle biosynthetic process' (Fig. 5G). Furthermore, KEGG signaling pathways such as classical pathway in cancer and MAPK pathways including NF-κB and JNK were also enriched (Fig. 5H). Western blotting assays confirmed that

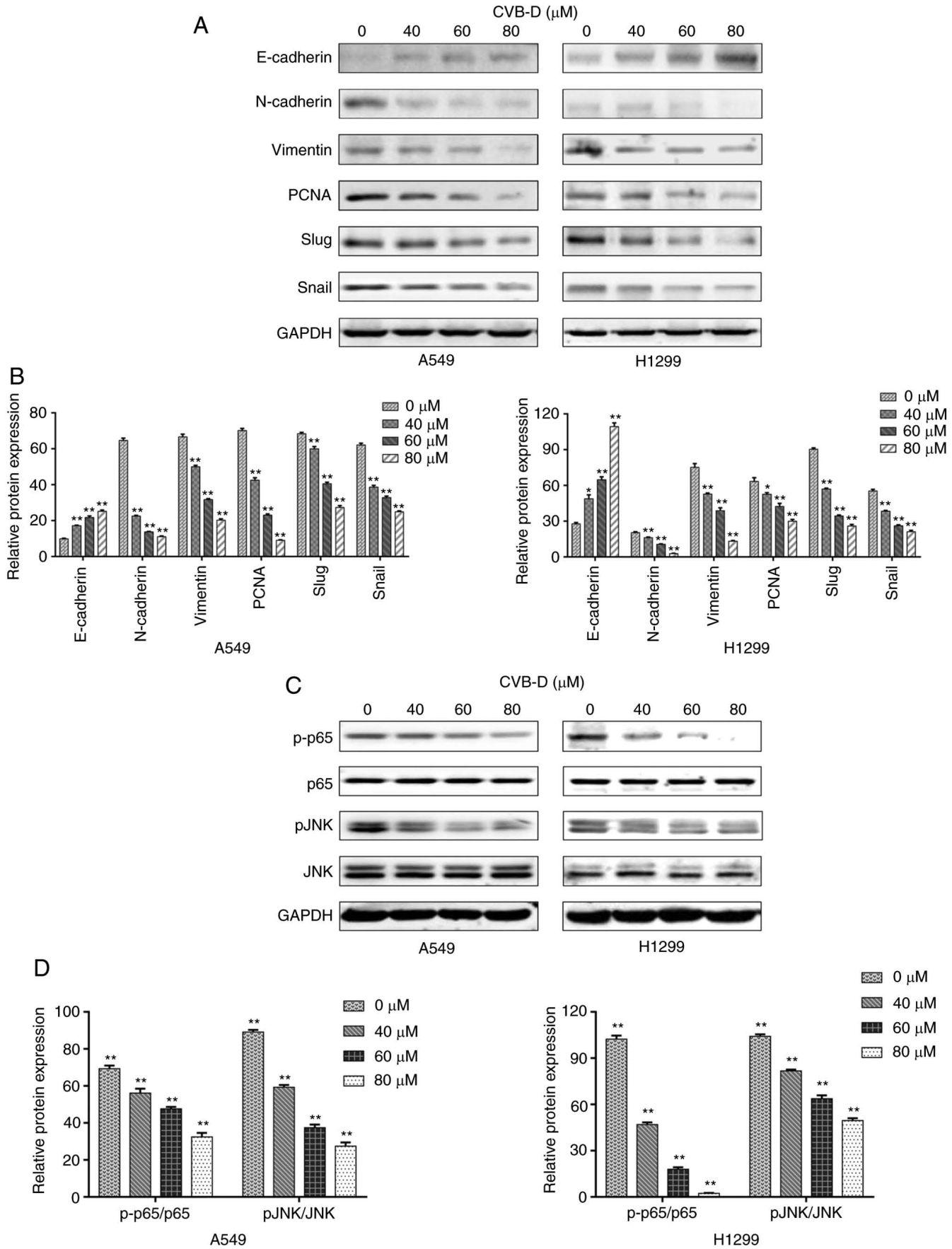

Figure 4. CVB-D treatment inhibits EMT in the NSCLC cells. (A and B) Western blot assay results revealed the levels of EMT-associated proteins (E-cadherin, vimentin and N-cadherin), proliferation marker protein (PCNA), and EMT-related transcriptional factors (Snail and Slug) in the control and CVB-D-treated NSCLC cells. (C and D) Western blot assay results showed the expression levels of the NF-κB/JNK signaling pathway proteins in the control and CVB-D-treated NSCLC cells. *P<0.05 and **P<0.01 vs. control. CVB-D, cyclovirobuxine D; NSCLC, non-small cell lung cancer; EMT, epithelial-to-mesenchymal transition; PCNA, proliferating cell nuclear antigen; p-, phosphorylated.

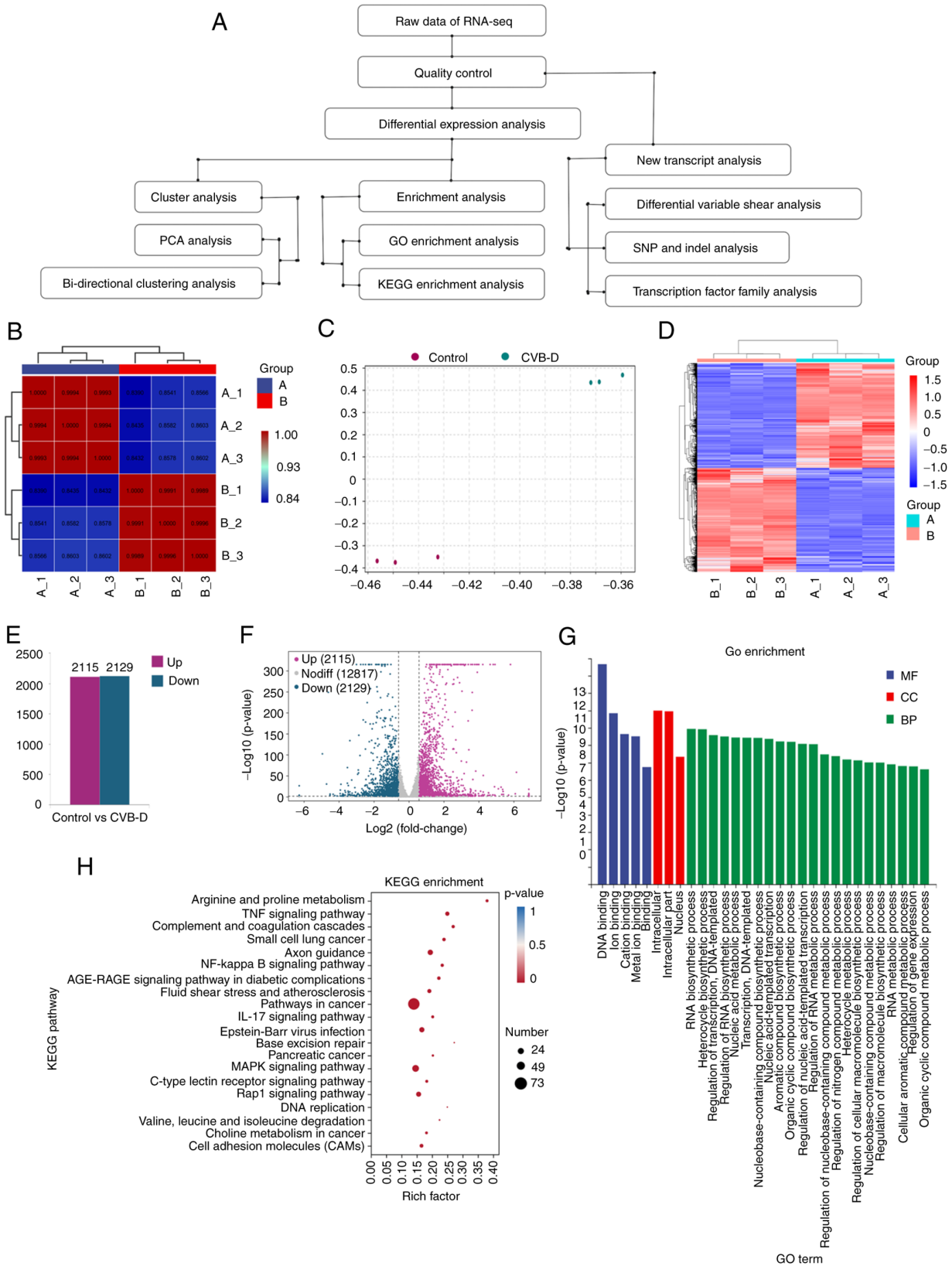

Figure 5. Transcriptome analysis of the RNA-sequencing data from the control and CVB-D-treated A549 cells. (A) Flowchart of the transcriptome analysis. (B) Pearson's correlation analysis of the gene expression patterns between the control and CVB-D-treated NSCLC samples. (C) PCA showed the grouping of control and CVB-D-treated NSCLC samples based on the transcriptome data. (D) Heatmap revealed the bidirectional cluster analysis of the DEGs between control and CVB-D-treated A549 cells. The upregulated and downregulated genes are highlighted in red and blue, respectively. (E) Distribution of the 2115 upregulated DEGs and 2129 downregulated DEGs in the CVB-D-treated A549 cells. (F) Volcano plots demonstrated the expression profiles of DEGs in the CVB-D treatment group compared with the control group, including the upregulated (purple), downregulated (green) and normally (gray) expressed genes. (G) GO enrichment analysis showed the enriched molecular function MF, CC and BP terms associated with the downregulated DEGs. (H) The bubble chart revealed enriched KEGG pathways related to the downregulated DEGs. CVB-D, cyclovirobuxine D; NSCLC, non-small cell lung cancer; PCA, principal component analysis; DEGs, differentially expressed genes; GO, Gene Ontology; MF, molecular function; CC, cellular component; BP, biological process; KEGG, Kyoto Encyclopedia of Genes and Genomes.

CVB-D treatment significantly decreased the expression levels of p-p65 (NF-kB) and p-JNK in a concentration-dependent manner (0, 40, 60, and 80 μM for 24 h) without altering total p65 and JNK expression levels (Fig. 4C and D). This suggested that CVB-D treatment inhibited the activation of NF-κB/JNK signaling pathway in the NSCLC cells.

CVB-D suppresses the KIF11-CDK1-CDC25C-CyclinB1 G_2/M phase transition regulatory network in the NSCLC cells. GEPIA 2 database analysis was performed based on two threshold parameters, namely, |log2FoldChange|>1 and P<0.05. The results showed that 1103 genes out of the 4245 overexpressed genes correlated with LUAD and 500 prognosis-associated DEGs correlated with OS and/or disease-free survival (DFS) rates of patients with LUAD. Furthermore, 5593 potential therapeutic target genes related to NSCLC were identified from the GeneCards database. The Ensembl-gene-IDs (beginning with 'ENSG') for the 2129 downregulated genes from the RNA-seq study were converted into standard-gene-symbols using the online gene ID conversion tool in the DAVID 6.8 database and the ENSEMBL database. Standard gene symbols were identified for 2111 out of 2129 downregulated genes but the gene symbols for the remaining 18 downregulated genes could not be identified. Comparative analysis of the 2111 downregulated genes, 1103 overexpressed genes in LUAD, and 5593 potential therapeutic target genes related to NSCLC identified 66 overlapping genes. In addition, 10 genes that correlated with the OS and/or DFS rates of LUAD patients were identified by comparative analysis of the 66 overlapping genes and the 500 prognosis-associated DEGs using the Venny online tool (Fig. 6A). The overexpression of these 10 genes in the GEPIA 2 LUAD patients' dataset and their associations with OS and/or DFS rates in the LUAD patients are shown in Figs. S3-S5.

A protein-protein interaction (PPI) network was constructed among these 10 DEG-encoded proteins using the String online database (Fig. 6B). It revealed close interactions between six proteins but the remaining four proteins did not show significant interactions. Therefore, the non-interacting nodes were excluded from the PPI network in Fig. 6B. The six interacting proteins were KIF11, CDK1, CDC25C, SKA1, KIF23 and ECT2. GeneCards database analysis demonstrated that the GeneCards Inferred Functionality Scores (GIFtS) for KIF11, CDK1 and CDC25C (46, 43 and 46, respectively) were higher than those GIFtS for SKA1, KIF23 and ECT2 (35, 42 and 39, respectively). Higher GIFtS predicted stronger degree of functionality. The 3 genes with higher GIFtS were associated with lower OS and/or DFS in patients with LUAD compared with those with lung squamous carcinoma. GEPIA 2 database analysis showed significantly higher correlation between KIF11 and CDK1 (r=0.8; P<0.001), KIF11 and CDC25C (r=0.74; P<0.001) and CDK1 and CDC25C (r=0.67; P<0.001) (Fig. S6). The correlation between KIF11 and CDK1 (r=0.8; P<0.001) was higher than the correlations between CDK1 and ECT2 (r=0.66; P<0.001), CDK1 and SKA1 (r=0.68; P<0.001), and CDK1 and KIF23 (r=0.77; P<0.001) (Fig. S7A). The correlation between KIF11 and CDC25C (r=0.74; P<0.001) was higher than the correlations between ECT2 and CDC25C (r=0.63; P<0.001) and KIF23 and CDC25C (r=0.72; P<0.001), and lower than the correlation between SKA1 and CDC25C (r=0.75; P<0.001) (Fig. S7B). The activation of CDK1 and its regulator CDC25C showed close correlation with G_2/M phase cell cycle arrest. The G_2 phase-related cyclinB1 is associated with the activation of CDK1 and CDC25C, and G_2/M cell cycle arrest. Therefore, in addition to CDC25C and CDK1, KIF11, KIF23, SKA1 and ECT2 were identified as potential CVB-D targets based on their correlation with cyclin B1.

The correlations between KIF23 and cyclinB1 (r=0.81; P<0.001), SKA1 and cyclin B1 (r=0.8; P<0.001), and ECT2 and cyclinB1 (r=0.67, P<0.001) were lower than the correlation between KIF11 and cyclinB1 (r=0.82; P<0.001) (Fig. S7C). Furthermore, the correlations between other transcription factors and the four potential CVB-D target genes, KIF11, KIF23, SKA1 and ECT2, were analyzed. The correlation of KIF11 with Bax, Bcl-2, PCNA, N-cadherin, E-cadherin, Slug, and Snail was low and there was no correlation between these factors and the other three genes, namely, KIF23, SKAI and ECT2 (Fig. S8). The expression levels of these six DEGs were then compared using the interactive heatmap from the GEPIA 2 database. KIF11 expression levels showed significant differences among the LUAD tumors and the normal lung tissues, but the differences in the expression levels of KIF23, SKAI and ECT2 between the LUAD tumors and the normal lung tissues were not significantly different (Fig. 6C). Therefore, KIF23, SKA1 and ECT2 were excluded. Furthermore, KIF11 and CDK1 were identified as the potential CVB-D target genes by comparative analysis of the 10 overlapping genes and the 100 predicted CVB-D-target genes from the Swisstarget prediction database (Fig. 6D).

Bioinformatics data analysis of the lung cancer patient data from several online databases demonstrated that the KIF11 protein and mRNA levels were significantly higher in the LUAD tissues compared with the adjacent normal lung tissues (Figs. S3 and S9A and B). HPA database analysis showed that KIF11 was an unfavorable prognostic marker in lung cancer; KIF11 protein expression was closely related to cell cycle regulation and KIF11 protein was mostly located in the cytosol and the mitotic spindle (Fig. S9C). KIF11 mRNA levels in the LUAD tissues ranked 17th among 31 types of tumors (Fig. S9D). KIF11 overexpression was associated with worse OS in LUAD (Fig. S9E). HPA and GEPIA 2 database analyses also demonstrated that CDK1, CDC25C, and cyclinB1 mRNA levels were significantly higher in the lung cancer tissues and were considered as unfavorable prognostic markers in patients with lung cancer (Figs. S3 and S9F). In patients with lung cancer, high expression levels of CDK1, CDC25C and cyclinB1 were associated with worse OS and DFS (Fig. S9E). The correlations between KIF11, CDK1, cyclinB1 genes and their 15 closest neighbors based on the tissue RNA-seq data are shown in Table SIII. Spearman's correlation coefficients between KIF11, CDK1, and cyclinB1 were close to 1. This demonstrated strong correlation between KIF11, CDK1 and cyclinB1 in cell cycle regulation.

Western blot analysis demonstrated that CVB-D treatment decreased the expression levels of KIF11, CDK1, CDC25C and cyclinB1 proteins in the A549 and H1299 cells in a concentration-dependent manner (Figs. 6E and S10A). IHC results demonstrated that the expression levels of KIF11 in the CVB-D group were significantly reduced compared with the control group (Fig. 6F and G). Western blot and RT-qPCR

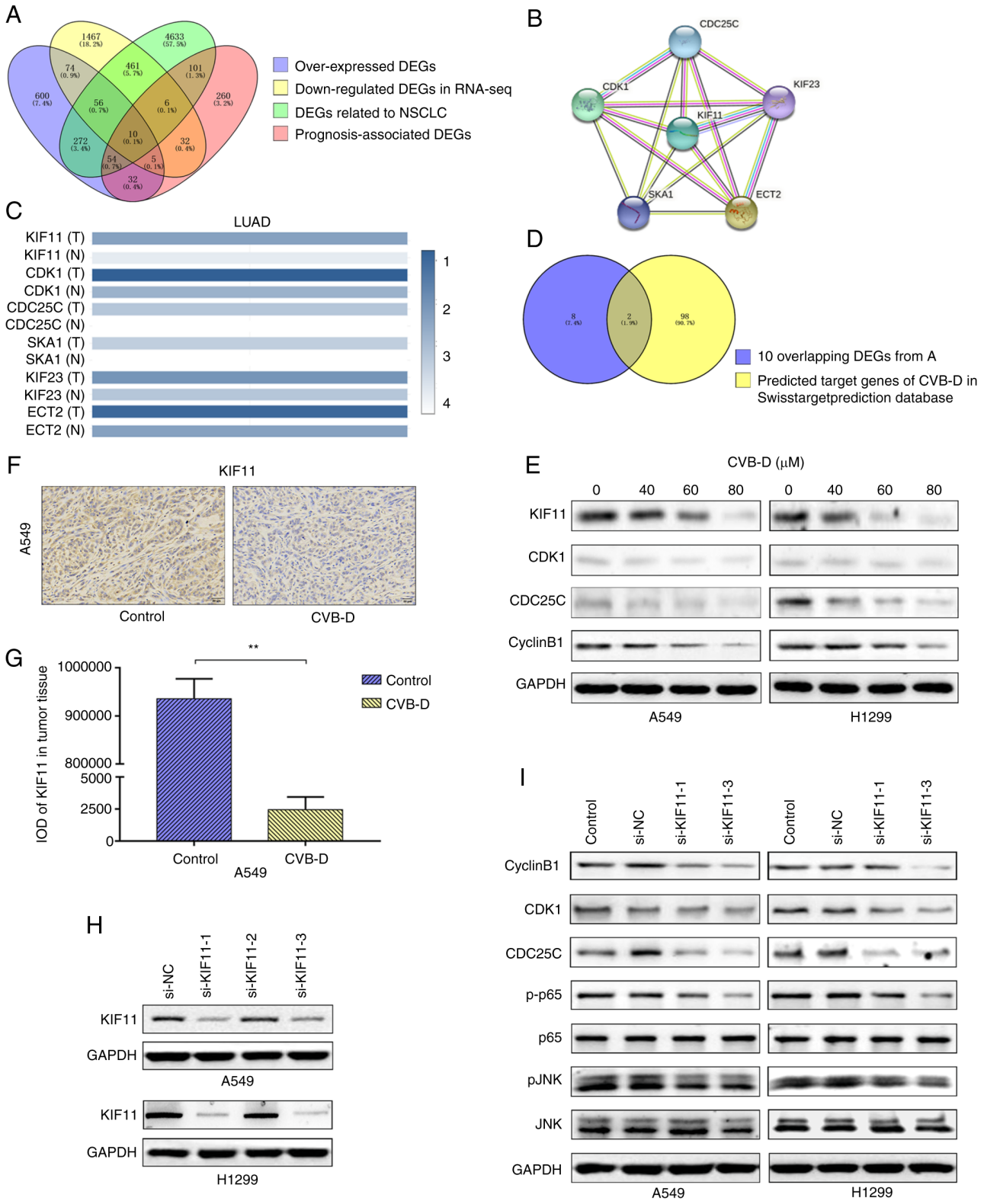

Figure 6. KIF11, KIF11-CDK1-CDC25C-cyclinB1 oncogenic network and NF-kB/JNK signaling pathway are the potential CVB-D therapeutic targets in the NSCLC cells. (A) Venn diagram showed the overlap number of potential CVB-D target genes in NSCLC cells by intersecting four LUAD datasets. (B) Protein-protein interaction network analysis revealed interaction between the 10 overlapping DEGs. The disconnected nodes are hidden. (C) The interactive heatmap from GEPIA 2 database showed expression of the 6 DEGs in LUAD and normal lung tissues. KIF11 is the most differentially expressed gene between LUAD and normal lung tissues. (D) Venn diagram revealed 2 common genes (KIF11 and CDK1) based on intersection between the 10 overlapping DEGs and the 100 predicted CVB-D target genes extracted from the Swisstarget prediction database. (E) Western blot analysis identified the expression of KIF11, CDK1, CDC25C and cyclinB1 proteins in the control and CVB-D-treated NSCLC cells. (F and G) Immunohistochemical assay results showed the expression levels and localization of the KIF11 protein in the control and CVB-D-treated A549 xenograft tumor tissues. (H) Western blot assay results revealed the KIF11 protein levels in the si-NC and si-KIF11-transfected NSCLC cells. (I) Western blot analysis demonstrated the expression levels of the oncogenic signaling network proteins (KIF11, CDK1, CDC25C and CyclinB1) and the NF-κB/JNK signaling pathway proteins (p65, p-p65, JNK and p-JNK) in the si-NC- and si-KIF11-transfected NSCLC cells. **P<0.01 vs. control group. KIF11, kinesin family member 11; CVB-D, cyclovirobuxine D; NSCLC, non-small cell lung cancer; LUAD, lung adenocarcinoma; DEGs, differentially expressed genes; si, small interfering; NC, negative control; p-, phosphorylated.

analyses revealed that transfection of si-KIF11-1 and si-KIF11-3 significantly reduced the levels of KIF11 protein and mRNA in the NSCLC cells (Figs. 6H; S10B and C). KIF11 silencing significantly reduced the expression levels of CDC25C, CDK1, p-p65/p65, p-JNK/JNK and cyclinB1 in the NSCLC cells (Figs. 6I and S10D). This suggested that KIF11 was upstream of the NF-κB/JNK signaling pathway. KIF11 knockdown partially rescued the growth inhibition of NSCLC cells by CVB-D (Fig. S10E). Then, the expression levels of KIF11, CDC25C and CDK1 were further analyzed in the cyclinB1-silenced NSCLC cells. Western blot results showed that transfection of si-cyclinB1-1 and si-cyclinB1-3 significantly reduced the levels of cyclinB1 protein in the NSCLC cells (Fig. S11A and B). CyclinB1 silencing significantly reduced the expression levels of KIF11, CDC25C and CDK1 protein levels in the NSCLC cells (Fig. S11C and D). This suggested that cyclinB1 regulated the KIF11-CDC25C-CDK1 G_2/M phase transition regulatory axis. Furthermore, these results suggested that CVB-D targeted the KIF11-CDC25C-CDK1-cyclinB1 G_2/M phase transition regulatory network in the NSCLC cells.

CVB-D inhibits in vivo progression of NSCLC tumors. Next, the *in vivo* therapeutic effects of CVB-D were evaluated in the A549 xenograft nude mice model (Fig. 7A). CVB-D treatment significantly inhibited xenograft tumor growth *in vivo*. The xenograft tumor weights and volumes were significantly lower in the CVB-D treatment group compared with the control group after 4 weeks (Fig. 7B-E). H&E staining demonstrated that CVB-D treatment significantly inhibited tumor growth and angiogenesis (Fig. 7F). TUNEL assay demonstrated that CVB-D treatment significantly increased apoptosis in the A549 xenograft tumors (Fig. 7F and G). The control and CVB-D-treated xenograft tumor-bearing nude mice did not exhibit any significant differences in the body weights (Fig. 7H). IHC staining analysis showed that CVB-D treatment significantly decreased the proportion of Ki67-positive cells in the xenograft tumors compared with the controls (Fig. 7I and J). This suggested that CVB-D treatment inhibited *in vivo* NSCLC cell proliferation. Furthermore, the expression levels of the anti-apoptotic Bcl-2 protein and the EMT-related N-cadherin protein were significantly decreased in the xenograft tumor tissues of the CVB-D treatment group compared with the controls (Fig. 7I and J). IHC analysis revealed reduced expression of KIF11, CDK1, CDC25C and cyclinB1 in the xenograft tumor tissues of the CVB-D treatment group compared with the controls (Figs. 6F, 7I and J). This suggested that CVB-D induced *in vivo* G_2/M phase cell cycle arrest of the NSCLC cells. The *in vivo* CVB-D treatment exerted significant anti-NSCLC effects with low cytotoxicity in the normal tissues; moreover, malignant lesions were not observed in the major organs including brain, heart, lung, liver, kidney spleen, gut and stomach during the 4-week CVB-D treatment in mice (Fig. S12).

USI is a non-invasive clinical imaging technology without any side effects and can systematically provide reliable information regarding the *in vivo* progression and therapeutic efficacy of tumor (27). Therefore, USI was used to evaluate the anti-NSCLC effects of CVB-D in the A549 xenograft nude mice. B-mode ultrasonography, USE, CDFI, CPA in the USI mode and MI were used to determine the tumor size, the hardness degree, the presence of angiogenesis, and microcalcifications, respectively. USI results (Fig. 8) showed that the average tumor size of the xenograft tumors was significantly decreased after CVB-D treatment. CDFI and CPA scans demonstrated that angiogenesis was reduced in the CVB-D treatment group compared with the control group. USE data demonstrated that the degree of tumor hardness, which is closely correlated with tumor malignancy, decreased after CVB-D treatment. Ultrasonic MI technique was used to characterize microcalcifications in the A549 xenograft nude mice. Ultrasonic MI data showed firefly signs and the presence of multiple hypoechoic areas indicating malignancy in the control group. However, firefly signs and hyperechoic areas were significantly reduced in the CVB-D group. These results demonstrated that CVB-D significantly inhibited growth and progression of NSCLC cell derived xenograft tumors in the nude mice.

Molecular docking indicates the binding between CVB-D and KIF11-CDC25C-CDK1-cyclinB1 network. Molecular docking, an established *in silico* structure-based method, has been widely used in drug discovery and prediction of the binding interfaces between a target protein (enzyme) and drug molecules (ligands) through molecular techniques (28). AutoDock Vina was used to perform molecular docking of CVB-D into the crystal structures of KIF11, CDC25C, CDK1 and cyclinB1. The affinity of the docking pose was -7.3, -7.0, -9.7 and -6.7 kcal/mol, respectively, which indicated that there were strong bindings between CVB-D and KIF11, CDC25C, CDK1 and cyclinB1 (Fig. 9).

Chemical structure and mechanism of action of CVB-D in NSCLC cells. The chemical structure and molecular formula of CVB-D is shown in Fig. 10. The experimental data in the present study demonstrated that CVB-D significantly reduced the survival, proliferation, migration and invasion of the NSCLC cells by negatively regulating the NF-κB/JNK signaling pathway. Furthermore, CVB-D induced G_2/M phase cell cycle arrest of the NSCLC cells through targeted inhibition of the oncogenic KIF11-CDC25C-CDK1-cyclinB1 G_2/M phase transition regulatory network. The schematic presentation of the anti-NSCLC effects of CVB-D and the underlying molecular mechanisms are demonstrated in Fig. 10.

Discussion

Lung cancer is the leading cause of cancer-related morbidity and mortality worldwide. Therefore, lung cancer research is a major focus area of research. NSCLC accounts for >80% of the lung cancer cases (29). Most patients with NSCLC are diagnosed with locally advanced or metastatic disease. Currently, there are no effective screening measures for diagnosing lung cancer in the preliminary stages. Furthermore, the prognosis of patients with advanced NSCLC is poor (30). In the last two decades, advances in medical technology have significantly improved our understanding of the pathogenic mechanisms underlying NSCLC growth and progression and have resulted in the development of novel therapies including small molecule-targeted antitumor drugs including tyrosine kinase inhibitors and immunotherapy. Despite these advances, the

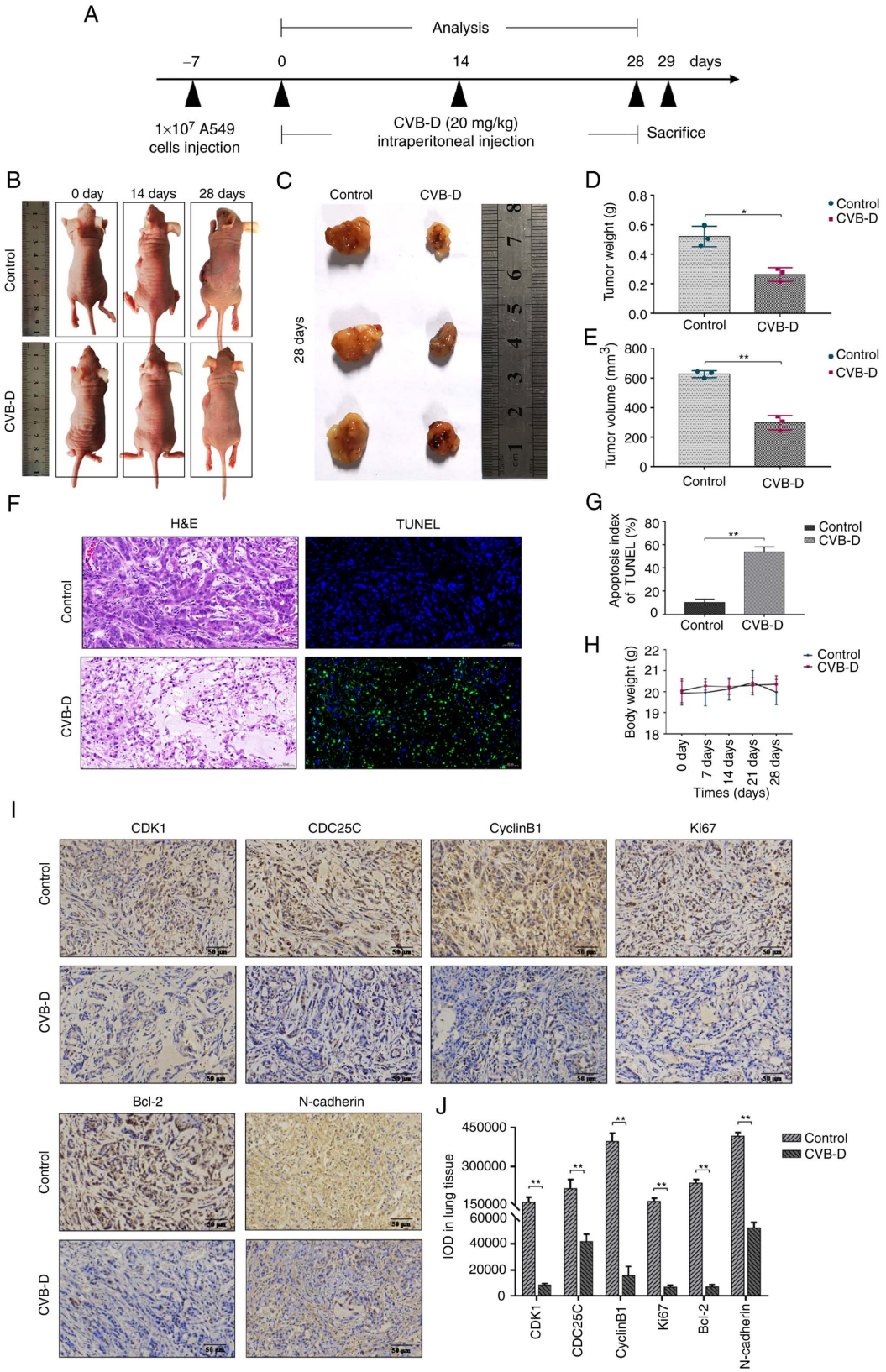

Figure 7. CVB-D inhibits *in vivo* progression of A549 xenografts tumors. (A) Experimental design for tumor xenograft experiments of NSCLC in nude mice to evaluate the *in vivo* therapeutic effects of CVB-D. Specific time points for CVB-D treatment and experimental analysis are indicated. (B) Representative images of the NSCLC xenograft tumor models with or without CVB-D treatment. (C) Representative images of the NSCLC xenograft tumor tissues from control and CVB-D-treated mice. (D and E) NSCLC xenograft tumor weights and volumes in the control and CVB-D treatment groups of nude mice. (F) Representative H&E and TUNEL staining images of the A549 xenograft tumor sections in the control and CVB-D treatment groups of nude mice (magnification, x200; scale bar, 50 μm). (G) The proportion of apoptotic cells in the A549 xenograft tumors derived from the control and CVB-D-treatment groups of nude mice based on TUNEL staining. (H) The body weights of the xenograft tumor model mice in the control and CVB-D treatment groups. (I and J) Immunohistochemical assay data revealed the expression levels and distribution of CDK1, CDC25C, cyclinB1, Ki67, Bcl-2 and N-cadherin proteins in the A549 xenograft tumors derived from the control and CVB-D treatment groups (magnification, x200; scale bar, 50 μm). *P<0.05 and **P<0.01 vs. control. CVB-D, cyclovirobuxine D; NSCLC, non-small cell lung cancer; H&E, hematoxylin and eosin.

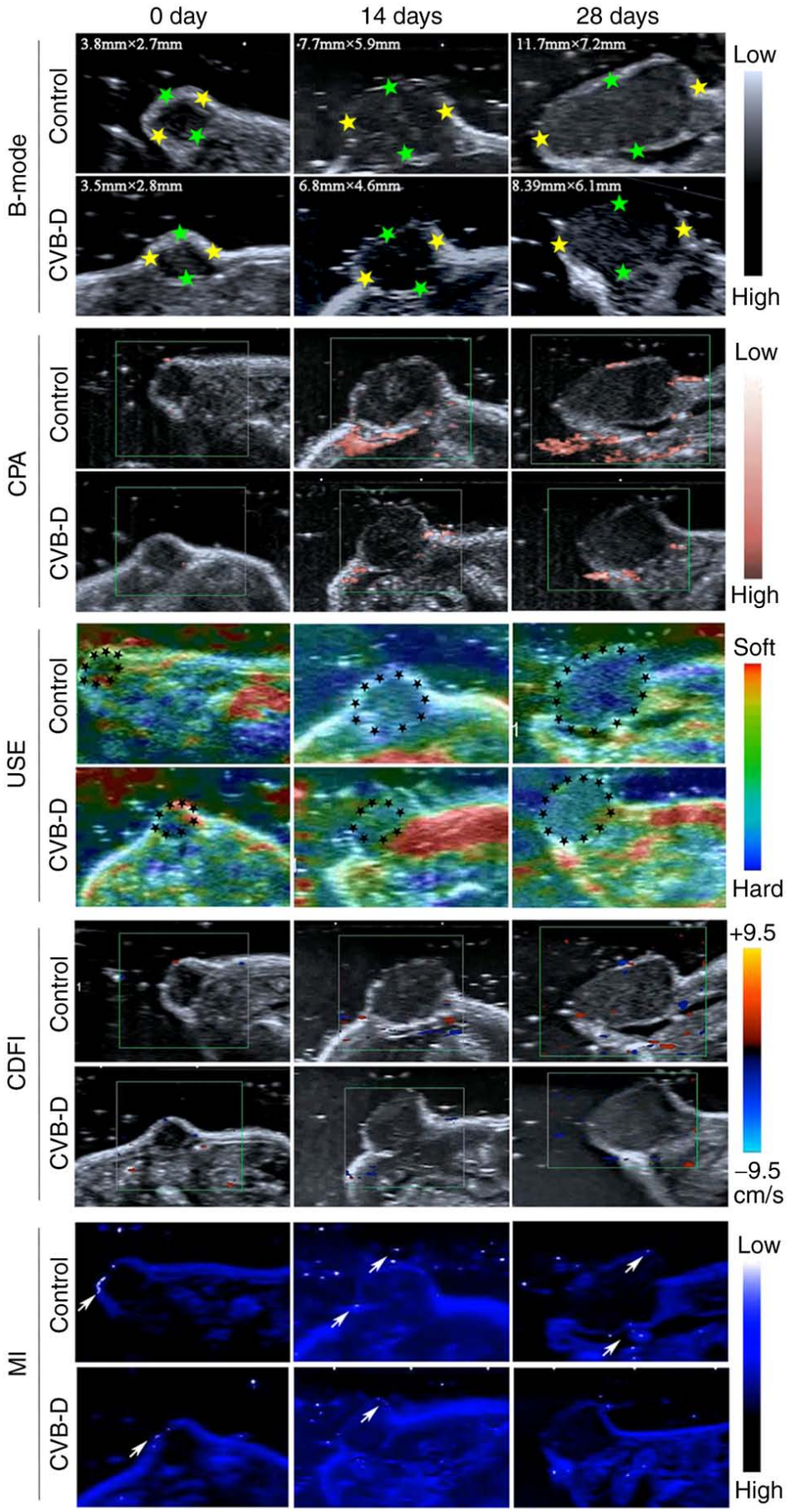

Figure 8. Ultrasonic imaging data of the non-small cell lung cancer xenograft tumors in the control and CVB-D treatment groups. This includes B-mode, CPA, USE, CDFI and MI. CVB-D, cyclovirobuxine D; B-mode, B-ultrasound; CPA, color power angiography; USE, ultrasonic elastosonography; CDFI, color Doppler flow imaging; MI, MicroPure Imaging.

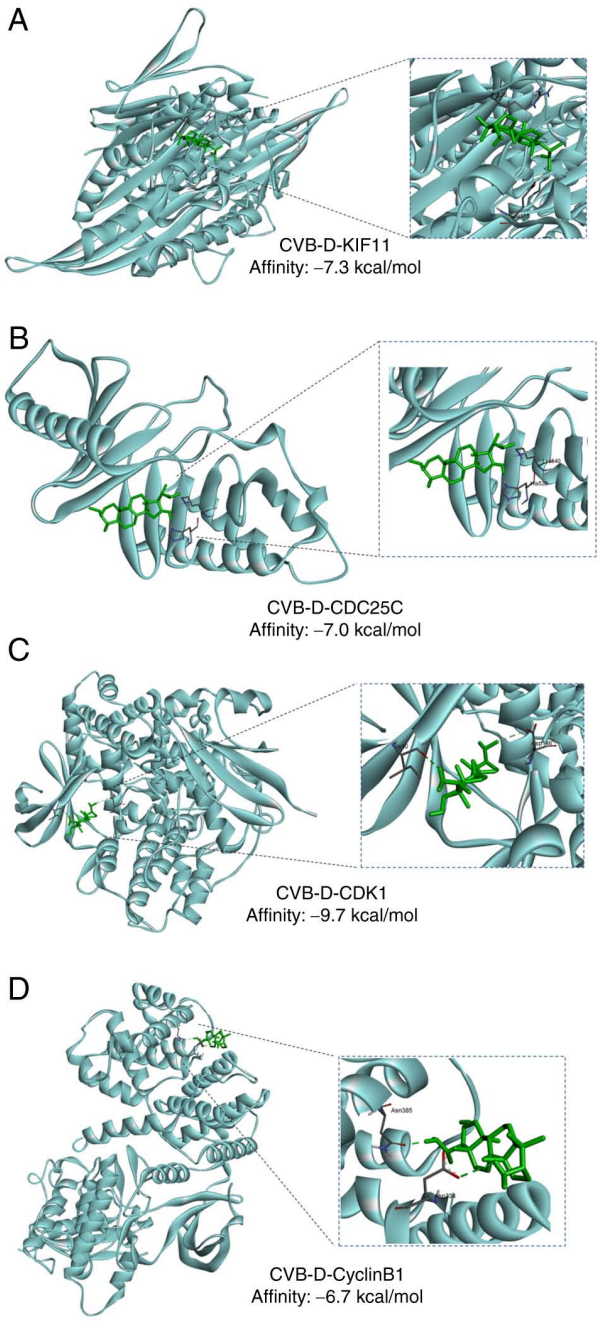

Figure 9. Molecular docking results of CVB-D in non-small cell lung cancer. (A-D) Molecular docking of CVB-D into the protein crystal structures of KIF11, CDC25C, CDK1 and cyclinB1. CVB-D, cyclovirobuxine D; KIF11, kinesin family member 11.

survival rates of patients with NSCLC remain significantly low, particularly for those with metastatic disease (31). Therefore, there is an urgent need for continued research and development of novel chemotherapeutic drugs and alternative agents with fewer side effects to improve the survival outcomes of patients with NSCLC. In the present study, the antitumor efficacy and underlying mechanisms of CVB-D, an NPC derived from *B. microphylla*, were investigated using the NSCLC nude mice model. Recent studies have demonstrated anticancer activities of CVB-D in multiple cancers (18-20). Furthermore, CVB-D induced mitophagy in the lung cancer cells by modulating the p65/BNIP3/LC3 signaling axis (21). However, to the best of our knowledge, the targets of CVB-D in the lung cancer cells have not been reported. In the present study, it was demonstrated that CVB-D inhibited NSCLC growth and progression by downregulating the MAPK/NF-κB signaling pathway. CVB-D also suppressed growth and progression of NSCLC cells by suppressing the KIF11-CDC25C-CDK1-cyclinB1 G_2/M phase transition regulatory network in the NSCLC cells.

EMT is closely associated with tumor invasion and metastasis, and resistance to chemotherapy and radiotherapy (32) in various cancers (16). The present study showed that CVB-D treatment inhibited EMT in the NSCLC cells based on the increased expression of E-cadherin and decreased expression of mesenchymal markers including N-cadherin and vimentin. Therefore, CVB-D is a potential therapeutic drug for inhibiting EMT and progression of NSCLC. Tumor metastasis is a characteristic feature of malignant tumors and is associated with poor prognosis since the cancer cells acquire migratory and invasive characteristics, leave the primary tumor site and establish metastasis at distant sites (33). In the current study, it was revealed that CVB-D suppressed migration and invasion of NSCLC cells in a concentration-dependent manner. the effects of CVB-D on the lung cancer cells, were evaluated both *in vitro* and *in vivo*, using different experimental approaches. CVB-D significantly reduced *in vitro* NSCLC cell proliferation, colony formation, survival and cell cycle progression in a dose-dependent manner. USI data showed that CVB-D treatment decreased *in vivo* angiogenesis. FCM analysis demonstrated that CVB-D induced G_2/M phase cell cycle arrest of the NSCLC cells. The expression levels of several pro-apoptotic and cell cycle-related transcription factors including Bcl-2, Bax and cyclinB1 were reduced by CVB-D treatment. Bioinformatics analysis identified that the expression levels of cyclinB1 were significantly higher in the LUAD tissues compared with the adjacent para-cancerous tissues. Moreover, high cyclinB1 expression was associated with tumor progression and shorter OS time. CyclinB1 plays a key role in mitosis by regulating cell cycle progression through the G_2/M phase (34). These results demonstrated that CVB-D was a potential therapy for NSCLC because it effectively inhibited EMT, migration and invasion, and G_2/M cell cycling of NSCLC cells.

RNA-seq data is extensively used in clinical research and therapy to identify pathogenic mechanisms in various cancers (35). RNA-seq data analysis and mining is used to identify drug targets and their mechanisms of action in the human cancer cells including identification of the oncogenic signaling pathways that are targeted by the antitumor agents (36). In the present study, RNA-seq data analysis showed that CVB-D treatment downregulated KIF11, CDC25C and CDK1 expression levels in the NSCLC cells.

RNA-seq data analysis identified KIF11 was the potential therapeutic target of CVB-D in the NSCLC cells. KIF11 plays a significant role in spindle formation. Previous studies have reported that KIF11 is an oncogene in glioblastoma, HCC, breast, gallbladder and colorectal cancers (6-8,37,38). Furthermore, high expression of KIF11 is associated with poor survival outcomes in NSCLC patients (11,39). Recently, Yang *et al* (40) performed robust rank aggregation analysis of several LUAD datasets and reported that KIF11 was a potential prognostic biomarker associated with LUAD development. Furthermore, RNA-seq analysis of paired LUAD and para-cancerous lung

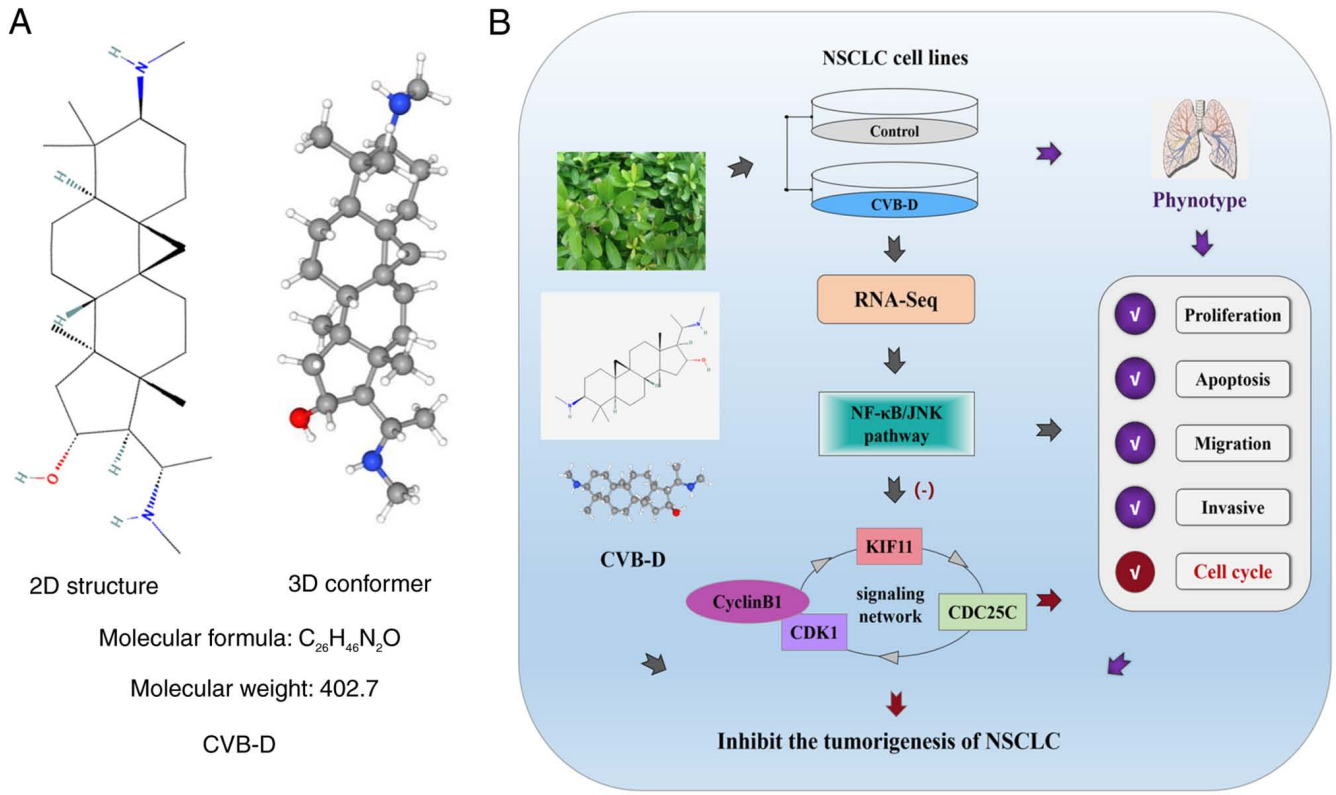

Figure 10. Chemical structure of CVB-D and its mechanism in the NSCLC cells. (A) The 2D structure and 3D conformation of CVB-D. (B) CVB-D inhibits NSCLC progression by suppressing activation of the NF-κB/JNK signaling pathway and the KIF11-CDK1-CDC25C-cyclinB1 network. CVB-D, cycloviro-buxine D; NSCLC, non-small cell lung cancer; KIF11, kinesin family member 11.

tissue samples resulted in the identification of eight enriched genes including KIF11 belonging to pathways related to cell division that were potential diagnostic and prognostic biomarkers for LUAD (41). Schneider *et al* (9) reported that five mitosis-related genes including KIF11 correlated with poor prognosis in NSCLC patients. Liu *et al* (39) evaluated The Cancer Genome Atlas-NSCLC datasets and demonstrated that high KIF11 expression was associated with lymph node metastases, advanced pathological stages and worse prognosis in patients with LUAD and NSCLC; moreover, multivariate analysis demonstrated that KIF11 was an independent prognostic factor for OS in patients with NSCLC. Wang *et al* (42) demonstrated that the expression levels of five DEGs including KIF11 correlated with the prognosis and progression of bladder cancer. Meng *et al* (43) and Gong *et al* (44) compared gene expression profiles of LUAD and NSCLC datasets in the Gene Expression Omnibus, Oncomine and GEPIA databases using functional enrichment, PPI network, DAVID, String, HPA and TfactS analyses and demonstrated that key cell cycle-related genes including KIF11 were potential biomarkers in lung cancer. Furthermore, several cell cycle-related genes including CDKs and KIF11 were downregulated by THZ1 treatment in the nasopharyngeal carcinoma cell lines; KIF11 expression correlated with THZ1-induced inhibition of nasopharyngeal carcinoma cell proliferation (45).

The inhibition of KIF11 by DHPMs significantly reduced growth, survival and progression of several breast cancer cell lines (46). Triple-negative breast cancer (TNBC) is an aggressive and highly heterogenous subtype that frequently develops resistance to chemotherapy and lacks effective treatment options. Jiang *et al* (47) reported that high expression of KIF11 in the $CD44^+/CD24^-$ subpopulation of docetaxel-resistant TNBC cells correlated with shorter DFS; KIF11 silencing suppressed TNBC cell proliferation, migration and invasion by inducing G_2/M cell cycle arrest and apoptosis in the docetaxel-resistant TNBC xenograft models; moreover, KIF11 inhibitor SB743921 significantly reduced docetaxel-resistant TNBC xenograft tumor growth. In another study, knockdown of KIF11 and Aurora Kinase A induced G_2/M cell cycle arrest in the TNBC cells; moreover, targeted inhibition of the Id1-KIF11 pathway combined with conventional chemotherapy achieved improved therapeutic effects for patients with TNBC (48). KIF11 knockdown significantly reduced proliferation of malignant pleural mesothelioma cells (49). The high expression of KIF11 in colorectal cancer correlated with advanced clinical tumor stages and vessel invasion; moreover, KIF11 knockdown inhibited growth and increased oxaliplatin sensitivity of colorectal tumor cells by activating p53 signaling and inhibiting GSK3β signaling (50). Furthermore, KIF11 is an independent prognostic factor in LUAD and is associated with poor OS and worse progression-free survival; KIF11 silencing significantly reduced proliferation, migration and invasion of LUAD cells and induced G_2/M cell cycle and apoptosis (11). Therefore, these data suggested that KIF11 is a potential oncogene and a promising therapeutic target in NSCLC. However, it remains to be evaluated if KIF11 inhibitors can be used as an alternative therapy to overcome resistance to conventional chemotherapeutics.

RNA-seq data also showed that CVB-D reduced CDC25C levels in the NSCLC cells. CDC25C is an important cyclin

that participates in the regulation of G_2/M progression by mediating DNA damage repair (51). Activation of the CDK1/cyclinB1 complex triggers mitosis and progression of the G_2/M cell cycle phase is regulated by CDC25C (52). DNA damage elicits signals that block mitosis by inhibiting the activation and nuclear import of CDK1/cyclinB1 (51,52). CDC25C plays a significant role in regulating checkpoint proteins and subsequent signal transduction to ensure accurate transmission of DNA information to the daughter cells (51,52). Downregulation of CDC25C in response to DNA damage induces cell cycle arrest in the G_2/M phase (51). Several studies have reported that aberrantly high expression of CDC25C in the lung, gastric, colon, breast and prostate cancers, is closely related with tumor growth and metastases, and poor prognosis; therefore, CDC25C is a useful diagnostic and prognostic biomarker in several malignant tumors (51).

RNA-seq data also revealed that CVB-D downregulated CDK1 in the NSCLC cells. CDK1 is an essential cell cycle regulatory protein that plays a key role in tumorigenesis and is considered as a promising target for cancer therapy. CyclinB1 is a regulatory subunit of CDK1, which promotes transition of cells from the G_2 phase into the mitosis (M) phase. The association of cyclinB1 with CDK1 is required for G_2 phase cells to enter into mitosis (24). The CDK1/cyclinB1 complex was considered as key regulatory proteins driving G_2 to M phase (24,53). CDC25C activates the CDK1/cyclinB1 complex and regulates the progression of the G_2/M cell cycle. Furthermore, in the G_2/M phase, positive feedback activation between CDC25C and CDK1/cyclinB1 promotes cell cycle progression through the G_2 checkpoint (51).

The association between KIF11, CDC25C, CDK1 and cyclinB1 was analyzed. The Venny online tool was used to analyze gene expression data of patients with NSCLC from the GEPIA 2 and GeneCards database and 10 overlapping DEGs were selected, which were all downregulated by CVB-D treatment in the RNA-seq data, overexpressed in LUAD tissues and associated with poor OS and/or DFS rates in patients with LUAD, and were recognized as therapeutic targets for NSCLC according to the GeneCards database. PPI network analysis of these 10 overlapping DEGs identified 6 closely related proteins including 3 oncogenes, namely, KIF11, CDK1 and CDC25C that exhibited high correlation with LUAD growth and progression. The present study demonstrated significant correlation between the expression levels of KIF11 and cyclinB1 in the NSCLC tissues and cells. Furthermore, Swisstarget prediction database analysis demonstrated that KIF11 and CDK1 were potential target genes of CVB-D. And then, these were verified by molecular docking. Finally, the KIF11-CDC25C-CDK1-cyclinB1 G_2/M transition regulatory network was identified as a potential target of CVB-D in the NSCLC cells.

RNA-seq data analysis demonstrated that CVB-D significantly inhibited JNK and NF-κB signaling pathways in the NSCLC cells. JNKs are MAPKs that transduce extracellular and intracellular stress and stimulatory signals that regulate cellular proliferation, differentiation, apoptosis, invasion, cell cycle arrest and malignant transformation (54-56). JNK activation promotes survival, proliferation and motility of HCC, ovarian cancer, and NSCLC cells (57-59). The inhibitors of JNK signaling pathway suppress cancer cell proliferation, survival, motility and malignancy. Therefore, JNK signaling pathway is an attractive target for cancer therapy. Previous studies have shown that inhibition of the JNK pathway suppressed the tumor cell viability, growth and progression of tumor cells by inducing cell cycle arrest and apoptosis (60,61). JNK pathway inhibitors such as SP600125 promote G_2/M cell cycle arrest and/or apoptosis of human breast carcinoma, HCC, NSCLC and melanoma cells (56,59,62-64). JNK activation is associated with cell cycle progression (60). NF-κB is a pleiotropic transcription factor and a key regulator of innate immune responses and multiple biological processes involved in cancer initiation, growth and progression (65,66). NF-κB signaling is constitutively activated in breast, gastric carcinoma, prostate, cervical, lung and pancreatic cancer tissues (67). Activation of the NF-κB signaling pathway correlates with increased proliferation, metastasis, angiogenesis and survival of cancer cells (67,68). Furthermore, increased NF-κB activity promotes cancer cell survival and drug resistance by upregulating anti-apoptotic genes (69).

The combination therapy with NF-κB pathway inhibitors and classical chemotherapeutics is more effective in treating malignancies compared with treatment with traditional chemotherapy (70). Therefore, NF-κB activation is an important target for effective treatment of several cancers. NF-κB inhibition improves the efficacy of several chemotherapeutics (67). NF-κB signaling pathway is the therapeutic target of several NPCs including poly phenols, flavonoids, terpenes, phenolics and alkaloids, which demonstrate anti-proliferative, pro-apoptotic, anti-angiogenic and anti-metastatic effects (67,68,71). Plant-derived anticancer agents including curcumin, baicalein and triptolide strongly inhibit NF-κB activation in the lung cancer cells, thereby confirming NF-κB is a key therapeutic target in lung cancer (67,71-73). Inhibition of NF-κB activity was shown by reduced levels of nuclear p-p65, the active form of NF-κB.

The results of the bioinformatics analysis were also confirmed by showing the inhibitory effects of CVB-D on the expression levels of KIF11, CDC25C, CDK1 and cyclinB1 proteins in the NSCLC cell lines using western blot analysis and in the subcutaneous tumor xenografts from the nude mouse model using IHC. The present study demonstrated that CVB-D inhibited NSCLC proliferation, metastasis, survival and cell cycle by suppressing NF-κB/JNK signaling, upregulating pro-apoptotic proteins such as Bax, inhibition of EMT-related proteins, downregulation of proliferation-related proteins including PCNA and cyclinB1, and suppression of anti-apoptotic factors such as Bcl-2. The present results also suggested that NF-κB and JNK signaling pathways acted upstream of the CDC25C-CDK1-cyclinB1 axis in the NSCLC cells and were consistent with the induction of G_2/M cell cycle arrest by CVB-D.

In the current study, it was also identified that si-RNA-mediated knockdown of KIF11 expression in the NSCLC cell lines decreased the levels CDC25C, CDK1 and cyclinB1, as well as p-JNK and p-p65. This suggested that KIF11 was upstream of the NF-κB/JNK pathway. Furthermore, to ascertain whether KIF11 mediated the therapeutic functions of CVB-D, rescue experiments were performed and it was revealed that the therapeutic effects of CVB-D were more effective in the KIF11-silenced NSCLC cells. Moreover, si-RNA-mediated

silencing of KIF11 partially reversed CVB-D-induced growth inhibition in the NSCLC cells. These results suggested that the antitumor effects of CVB-D in the NSCLC cells were mediated by suppression of the KIF11-CDC25C-CDK1-cyclinB1 G_2/M phase transition regulatory axis. Furthermore, the antitumor mechanism of CVB-D was a KIF11-dependent mechanism with CDC25C/CDK1/cyclinB1 acting as could be downstream targets of KIF11.

Lastly, the antitumor effects of CVB-D were further corroborated through the KIF11-CDC25C-CDK1-cyclinB1 G_2/M phase transition regulatory axis by evaluating the expression levels of KIF11, CDC25C and CDK1 in cyclinB1-silenced NSCLC cells. CyclinB1 silencing significantly reduced the expression levels of KIF11 CDC25C, and CDK1. This was consistent with the results of a previous study by Saijo *et al* (74) that showed significant correlation between the expression levels of KIF11 and cyclinB1. It was postulated by the authors that the knockdown of cyclinB1 disrupted the formation of the CDK1/cyclinB1 complex that was required for transitioning from G_2 phase into the mitotic phase, thereby resulting in G_2/M phase arrest. Moreover, cyclinB1 silencing downregulated the expression of a key G_2/M regulatory protein CDC25C. Hence, KIF11, CDC25C and CDK1 contributed to the G_2/M phase cell cycle arrest of cyclinB1-silenced NSCLC cells. Additionally, this suggested that the KIF11-CDC25C-CDK1 signaling axis was regulated by cyclinB1. These findings also showed the positive regulatory loop of the KIF11-CDC25C-CDK1-cyclinB1 signaling axis, which is a potential therapeutic target of CVB-D in the NSCLC cells.

Currently, platinum compounds including cisplatin and carboplatin are the first-line chemo therapeutics for patients with NSCLC either alone or in combination with other therapies. However, resistance to platinum therapeutics is a major cause of relapse in a large proportion of patients with NSCLC. Chemotherapeutic resistance is caused by alterations in pathways that regulate apoptosis, hypoxia, EMT and metabolism (75). Therefore, therapeutic strategies for relapsed NSCLC patients include therapies that induce tumor cell apoptosis through upregulation of Bax and inhibition of Bcl-2, inhibition of hypoxia, glycolytic metabolism and EMT, as well as suppression of oncogenic signaling pathways including MAPK/JNK and NF-κB (75-77), and increase the sensitivity to cisplatin. Paclitaxel (PTX) is a first-line drug for the treatment of advanced patients with NSCLC. However, advanced stage NSCLC patients eventually develop resistance to prolonged treatment with PTX. Previous studies reported that PTX resistance of NSCLC cells can be overcome by downregulating the anti-apoptotic proteins, upregulating the pro-apoptotic proteins, and inhibiting the expression of drug-resistance genes and EMT-related genes, which are regulated by the NF-κB/MAPKs signaling pathways (78-80). Furthermore, interference with spindle formation improves the PTX susceptibility of NSCLC cells (78). KIF11 plays a significant role in spindle formation. KIF11 inhibitors overcome adverse effects associated with classical microtubule-targeting agents such as PTX, and show potential to overcome resistance to PTX (5). KIF11 inhibitors also sensitize NSCLC cells that are resistant to trametinib (MEK1/2 inhibitor) and induce anti-proliferative and anti-angiogenesis effects by inhibiting spindle formation during cell division (5). These data suggested that KIF11 is a promising therapeutic target. Therefore, future pre-clinical and clinical studies are required to test the efficacy of KIF11 inhibitors as later-line therapy of relapsed NSCLC patients or in combination with first-line chemotherapeutics for the treatment of newly diagnosed NSCLC patients.

This is an era of precision medicine and significant advances have been reported regarding the use of nanoparticles (NPs) to ensure efficient and safe delivery of chemotherapeutic antitumor drugs to specific tumor sites (81). Therefore, in the future, NPs loaded with CVB-D may be effective for treating a broad category of patients with NSCLC.

There are certain limitations to the present study. First, the sample size of the lung cancer xenograft nude mice model was small due to animal ethics limitations. However, despite this issue, the experimental results were consistent. Second, the differences in the efficiency of the siRNAs against KIF11 and cyclinB1 may be due to off-target effects.

In summary, it was demonstrated that CVB-D, a natural steroidal alkaloid, was highly effective in suppressing the *in vitro* and *in vivo* growth, survival and progression of NSCLC cells by inducing G_2/M phase cell cycle arrest and apoptosis. RNA-seq data analysis and *in vitro* and *in vivo* experiments demonstrated that CVB-D inhibited the KIF11-CDC25C-CDK1-cyclinB1 G_2/M phase transition regulatory network and the NF-κB/JNK signaling pathway. Therefore, the present study demonstrated that CVB-D was a promising targeted therapy for lung cancer.

Acknowledgements

Not applicable.

Funding

The present study was supported by the Basic Research Projects of Natural Sciences in Shanxi (grant. no. 20210302124039), the Scientific and Technological Innovation Programs of Higher Education Institutions in Shanxi (grant nos. 2020L0201 and 2020L0223), the National Natural Scientific Foundation of China (grant. nos. 32200168 and 82001850) and the Start-up Foundation for Doctoral Scientific Research of Shanxi Medical University (grant. no. XD1905).

Availability of data and materials

The datasets used and/or analyzed in the present study are available from the corresponding author on reasonable request. The original RNA-seq data in the present study has been deposited in the NCBI Sequence Read Archive (SRA) with the associated accession number PRJNA861972.

Authors' contributions

TX and YC conceived and designed the study. TX performed most of the experiments. YC and TX performed the USI experiments. JX guided the experiments related to the phenotype of cells. WD and TX performed the pathology experiments. PK guided the experiments related to IHC. TX analyzed the data and wrote the manuscript. XZ and PK reviewed and

revised the manuscript. TX, YC and XZ supervised the project and provided funding. TX and YC confirm the authenticity of all the raw data. All authors read and approved the final manuscript.

Ethics approval and consent to participate

All the animal experiments and protocols were approved (approval no. 2021-114) by the Animal Ethics Committee of the First Hospital of Shanxi Medical University (Taiyuan, China) and were conducted according to the national regulations in China.

Patient consent for publication

Not applicable.

Competing interests

The authors declare that they have no competing interests.

References

1. Bray F, Ferlay J, Soerjomataram I, Siegel RL, Torre LA and Jemal A: Global cancer statistics 2018: GLOBOCAN estimates of incidence and mortality worldwide for 36 cancers in 185 countries. CA Cancer J Clin 68: 394-424, 2018.
2. Inamura K: Lung Cancer: Understanding its molecular pathology and the 2015 WHO Classification. Front Oncol 7: 193, 2017.
3. Travis WD, Brambilla E, Burke AP, Marx A and Nicholson AG: Introduction to the 2015 World Health Organization Classification of tumors of the lung, pleura, thymus, and heart. J Thorac Oncol 10: 1240-1242, 2015.
4. Liu WJ, Du Y, Wen R, Yang M and Xu J: Drug resistance to targeted therapeutic strategies in Non-small cell lung cancer. Pharmacol Ther 206: 107438, 2020.
5. Garcia-Saez I and Skoufias DA: Eg5 targeting agents: From new anti-mitotic based inhibitor discovery to cancer therapy and resistance. Biochem Pharmacol 184: 114364, 2021.
6. Wei D, Rui B, Qingquan F, Chen C, Ping HY, Xiaoling S, Hao W and Jun G: KIF11 promotes cell proliferation via ERBB2/PI3K/AKT signaling pathway in gallbladder cancer. Int J Biol Sci 17: 514-526, 2021.
7. Neska-Dlugosz I, Buchholz K, Durslewicz J, Gagat M, Grzanka D, Tojek K and Klimaszewska-Wisniewska A: Prognostic impact and functional annotations of KIF11 and KIF14 expression in patients with colorectal cancer. Int J Mol Sci 22: 9732, 2021.
8. Li TF, Zeng HJ, Shan Z, Ye RY, Cheang TY, Zhang YJ, Lu SH, Zhang Q, Shao N and Lin Y: Overexpression of kinesin superfamily members as prognostic biomarkers of breast cancer. Cancer Cell Int 20: 123, 2020.
9. Schneider MA, Christopoulos P, Muley T, Warth A, Klingmueller U, Thomas M, Herth FJ, Dienemann H, Mueller NS, Theis F and Meister M: AURKA, DLGAP5, TPX2, KIF11 and CKAP5: Five specific mitosis-associated genes correlate with poor prognosis for non-small cell lung cancer patients. Int J Oncol 50: 365-372, 2017.
10. Fu F, Zhang Y, Gao Z, Zhao Y, Wen Z, Han H, Li Y and Chen H: Development and validation of a five-gene model to predict postoperative brain metastasis in operable lung adenocarcinoma. Int J Cancer 147: 584-592, 2020.
11. Li Z, Yu B, Qi F and Li F: KIF11 Serves as an independent prognostic factor and therapeutic target for patients with lung adenocarcinoma. Front Oncol 11: 670218, 2021.
12. Liu X, Liu X, Li J and Ren F: Identification and integrated analysis of key biomarkers for diagnosis and prognosis of non-small cell lung cancer. Med Sci Monit 25: 9280-9289, 2019.
13. Wang Z, Ma L, Su M, Zhou Y, Mao K, Li C, Peng G, Zhou C, Shen B and Dou J: Baicalin induces cellular senescence in human colon cancer cells via upregulation of DEPP and the activation of Ras/Raf/MEK/ERK signaling. Cell Death Dis 9: 217, 2018.
14. Pricci M, Girardi B, Giorgio F, Losurdo G, Ierardi E and Di Leo A: Curcumin and colorectal cancer: From basic to clinical evidences. Int J Mol Sci 21: 2364, 2020.
15. Rauf A, Imran M, Butt MS, Nadeem M, Peters DG and Mubarak MS: Resveratrol as an anti-cancer agent: A review. Crit Rev Food Sci Nutr 58: 1428-1447, 2018.
16. Erin N, Grahovac J, Brozovic A and Efferth T: Tumor microenvironment and epithelial mesenchymal transition as targets to overcome tumor multidrug resistance. Drug Resist Updat 53: 100715, 2020.
17. Jiang Z, Fu L, Xu Y, Hu X, Yang H, Zhang Y, Luo H, Gan S, Tao L, Liang G and Shen X: Cyclovirobuxine D protects against diabetic cardiomyopathy by activating Nrf2-mediated antioxidant responses. Sci Rep 10: 6427, 2020.
18. Zhou L, Tang H, Wang F, Ou S, Wu T, Fang Y, Xu J and Guo K: Cyclovirobuxine D inhibits cell proliferation and migration and induces apoptosis in human glioblastoma multiforme and lowgrade glioma. Oncol Rep 43: 807-816, 2020.
19. Zhang J, Chen Y, Lin J, Jia R, An T, Dong T, Zhang Y and Yang X: Cyclovirobuxine D exerts anticancer effects by suppressing the EGFR-FAK-AKT/ERK1/2-slug signaling pathway in human hepatocellular carcinoma. DNA Cell Biol 39: 355-367, 2020.
20. Jiang F, Chen Y, Ren S, Li Z, Sun K, Xing Y, Zhu Y and Piao D: Cyclovirobuxine D inhibits colorectal cancer tumorigenesis via the CTHRC1AKT/ERKSnail signaling pathway. Int J Oncol 57: 183-196, 2020.
21. Zeng C, Zou T, Qu J, Chen X, Zhang S and Lin Z: Cyclovirobuxine D Induced-mitophagy through the p65/BNIP3/LC3 axis potentiates its apoptosis-inducing effects in lung cancer cells. Int J Mol Sci 22: 5820, 2021.
22. Livak KJ and Schmittgen TD: Analysis of relative gene expression data using real-time quantitative PCR and the 2(-Delta Delta C(T)) method. Methods 25: 402-408, 2001.
23. Creamer-Hente MA, Lao FK, Dragos ZP and Waterman LL: Sex- and strain-related differences in the stress response of mice to CO_2 euthanasia. J Am Assoc Lab Anim Sci 57: 513-519, 2018.
24. Xie B, Wang S, Jiang N and Li JJ: Cyclin B1/CDK1-regulated mitochondrial bioenergetics in cell cycle progression and tumor resistance. Cancer Lett 443: 56-66, 2019.
25. Cardano M, Tribioli C and Prosperi E: Targeting proliferating cell nuclear antigen (PCNA) as an effective strategy to inhibit tumor cell proliferation. Curr Cancer Drug Targets 20: 240-252, 2020.
26. Brabletz S, Schuhwerk H, Brabletz T and Stemmler MP: Dynamic EMT: A multi-tool for tumor progression. EMBO J 40: e108647, 2021.
27. Chen Y, Liu P, Sun P, Jiang J, Zhu Y, Dong T, Cui Y, Tian Y, An T, Zhang J, *et al*: Oncogenic MSH6-CXCR4-TGFB1 feedback loop: A novel therapeutic target of photothermal therapy in glioblastoma multiforme. Theranostics 9: 1453-1473, 2019.
28. Pinzi L and Rastelli G: Molecular docking: Shifting paradigms in drug discovery. Int J Mol Sci 20: 4331, 2019.
29. Socinski MA, Obasaju C, Gandara D, Hirsch FR, Bonomi P, Bunn P, Kim ES, Langer CJ, Natale RB, Novello S, *et al*: Clinicopathologic features of advanced squamous NSCLC. J Thorac Oncol 11: 1411-1422, 2016.
30. Duma N, Santana-Davila R and Molina JR: Non-small cell lung cancer: Epidemiology, screening, diagnosis, and treatment. Mayo Clin Proc 94: 1623-1640, 2019.
31. Herbst RS, Morgensztern D and Boshoff C: The biology and management of non-small cell lung cancer. Nature 553: 446-454, 2018.
32. Pastushenko I and Blanpain C: EMT Transition states during tumor progression and metastasis. Trends Cell Biol 29: 212-226, 2019.
33. Majidpoor J and Mortezaee K: Steps in metastasis: An updated review. Med Oncol 38: 3, 2021.
34. Gavet O and Pines J: Progressive activation of CyclinB1-Cdk1 coordinates entry to mitosis. Dev Cell 18: 533-543, 2010.
35. Hong M, Tao S, Zhang L, Diao LT, Huang X, Huang S, Xie SJ, Xiao ZD and Zhang H: RNA sequencing: New technologies and applications in cancer research. J Hematol Oncol 13: 166, 2020.
36. Paczkowska M, Barenboim J, Sintupisut N, Fox NS, Zhu H, Abd-Rabbo D, Mee MW, Boutros PC, Drivers P; PCAWG Drivers and Functional Interpretation Working Group, *et al*: Integrative pathway enrichment analysis of multivariate omics data. Nat Commun 11: 735, 2020.
37. Venere M, Horbinski C, Crish JF, Jin X, Vasanji A, Major J, Burrows AC, Chang C, Prokop J, Wu Q, *et al*: The mitotic kinesin KIF11 is a driver of invasion, proliferation, and self-renewal in glioblastoma. Sci Transl Med 7: 304ra143, 2015.
38. Hu ZD, Jiang Y, Sun HM, Wang JW, Zhai LL, Yin ZQ and Yan J: KIF11 promotes proliferation of hepatocellular carcinoma among patients with liver cancers. Biomed Res Int 2021: 2676745, 2021.

39. Liu J, Tian Y, Yi L, Gao Z, Lou M and Yuan K: High KIF11 expression is associated with poor outcome of NSCLC. Tumori 108: 40-46, 2022.
40. Yang Y, Zhang S and Guo L: Characterization of cell cycle-related competing endogenous RNAs using robust rank aggregation as prognostic biomarker in lung adenocarcinoma. Front Oncol 12: 807367, 2022.
41. Li S, Xuan Y, Gao B, Sun X, Miao S, Lu T, Wang Y and Jiao W: Identification of an eight-gene prognostic signature for lung adenocarcinoma. Cancer Manag Res 10: 3383-3392, 2018.
42. Wang L, Chen S, Luo Y, Yuan L, Peng T, Qian K, Liu X, Xiao Y and Wang X: Identification of several cell cycle relevant genes highly correlated with the progression and prognosis of human bladder urothelial tumor. J Cell Physiol 234: 13439-13451, 2019.
43. Meng F, Zhang L, Ren Y and Ma Q: Transcriptome analysis reveals key signature genes involved in the oncogenesis of lung cancer. Cancer Biomark 29: 475-482, 2020.
44. Gong K, Zhou H, Liu H, Xie T, Luo Y, Guo H, Chen J, Tan Z, Yang Y and Xie L: Identification and integrate analysis of key biomarkers for diagnosis and prognosis of non-small cell lung cancer based on bioinformatics analysis. Technol Cancer Res Treat 20: 15330338211060202, 2021.
45. Gao L, Xia S, Zhang K, Lin C, He X and Zhang Y: Gene expression profile of THZ1-treated nasopharyngeal carcinoma cell lines indicates its involvement in the inhibition of the cell cycle. Transl Cancer Res 10: 445-460, 2021.
46. Guido BC, Ramos LM, Nolasco DO, Nobrega CC, Andrade BY, Pic-Taylor A, Neto BA and Correa JR: Impact of kinesin Eg5 inhibition by 3,4-dihydropyrimidin-2(1H)-one derivatives on various breast cancer cell features. BMC Cancer 15: 283, 2015.
47. Jiang M, Zhuang H, Xia R, Gan L, Wu Y, Ma J, Sun Y and Zhuang Z: KIF11 is required for proliferation and self-renewal of docetaxel resistant triple negative breast cancer cells. Oncotarget 8: 92106-92118, 2017.
48. Thankamony AP, Murali R, Karthikeyan N, Varghese BA, Teo WS, McFarland A, Roden DL, Holliday H, Konrad CV, Cazet A, *et al*: Targeting the Id1-Kif11 Axis in triple-negative breast cancer using combination therapy. Biomolecules 10: 1295, 2020.
49. Kato T, Lee D, Wu L, Patel P, Young AJ, Wada H, Hu HP, Ujiie H, Kaji M, Kano S, *et al*: Kinesin family members KIF11 and KIF23 as potential therapeutic targets in malignant pleural mesothelioma. Int J Oncol 49: 448-456, 2016.
50. Zhou Y, Yang L, Xiong L, Wang K, Hou X, Li Q, Kong F, Liu X and He J: KIF11 is upregulated in colorectal cancer and silencing of it impairs tumor growth and sensitizes colorectal cancer cells to oxaliplatin via p53/GSK3beta signaling. J Cancer 12: 3741-3753, 2021.
51. Liu K, Zheng M, Lu R, Du J, Zhao Q, Li Z, Li Y and Zhang S: The role of CDC25C in cell cycle regulation and clinical cancer therapy: A systematic review. Cancer Cell Int 20: 213, 2020.
52. Takizawa CG and Morgan DO: Control of mitosis by changes in the subcellular location of cyclin-B1-Cdk1 and Cdc25C. Curr Opin Cell Biol 12: 658-665, 2000.
53. Wang JN, Zhang ZR, Che Y, Yuan ZY, Lu ZL, Li Y, Li N, Wan J, Sun HD, Sun N, *et al*: Acetyl-macrocalin B, an ent-kaurane diterpenoid, initiates apoptosis through the ROS-p38-caspase 9-dependent pathway and induces G2/M phase arrest via the Chk1/2-Cdc25C-Cdc2/cyclin B axis in non-small cell lung cancer. Cancer Biol Ther 19: 609-621, 2018.
54. Wu Q, Wu W, Jacevic V, Franca TCC, Wang X and Kuca K: Selective inhibitors for JNK signalling: A potential targeted therapy in cancer. J Enzyme Inhib Med Chem 35: 574-583, 2020.
55. Bubici C and Papa S: JNK signalling in cancer: In need of new, smarter therapeutic targets. Br J Pharmacol 171: 24-37, 2014.
56. Abdelrahman KS, Hassan HA, Abdel-Aziz SA, Marzouk AA, Narumi A, Konno H and Abdel-Aziz M: JNK signaling as a target for anticancer therapy. Pharmacol Rep 73: 405-434, 2021.
57. Song W, Ma Y, Wang J, Brantley-Sieders D and Chen J: JNK signaling mediates EPHA2-dependent tumor cell proliferation, motility, and cancer stem cell-like properties in non-small cell lung cancer. Cancer Res 74: 2444-2454, 2014.
58. Dou Y, Jiang X, Xie H, He J and Xiao S: The Jun N-terminal kinases signaling pathway plays a 'seesaw' role in ovarian carcinoma: A molecular aspect. J Ovarian Res 12: 99, 2019.
59. Wang J and Tai G: Role of C-Jun N-terminal kinase in hepatocellular carcinoma development. Target Oncol 11: 723-738, 2016.
60. Gutierrez GJ, Tsuji T, Cross JV, Davis RJ, Templeton DJ, Jiang W and Ronai ZA: JNK-mediated phosphorylation of Cdc25C regulates cell cycle entry and G(2)/M DNA damage checkpoint. J Biol Chem 285: 14217-14228, 2010.
61. Udden SN, Kwak YT, Godfrey V, Khan MAW, Khan S, Loof N, Peng L, Zhu H and Zaki H: NLRP12 suppresses hepatocellular carcinoma via downregulation of cJun N-terminal kinase activation in the hepatocyte. Elife 8: e40396, 2019.
62. Han YH, Mun JG, Jeon HD, Park J, Kee JY and Hong SH: Gomisin A ameliorates metastatic melanoma by inhibiting AMPK and ERK/JNK-mediated cell survival and metastatic phenotypes. Phytomedicine 68: 153147, 2020.
63. Okada M, Shibuya K, Sato A, Seino S, Watanabe E, Suzuki S, Seino M and Kitanaka C: Specific role of JNK in the maintenance of the tumor-initiating capacity of A549 human non-small cell lung cancer cells. Oncol Rep 30: 1957-1964, 2013.
64. Cheng J, Li M, Tzeng CM, Gou X and Chen S: Suppression of tumorigenicity 5 ameliorates tumor characteristics of invasive breast cancer cells via ERK/JNK Pathway. Front Oncol 11: 621500, 2021.
65. Baud V and Karin M: Is NF-kappaB a good target for cancer therapy? Hopes and pitfalls. Nat Rev Drug Discov 8: 33-40, 2009.
66. Hoesel B and Schmid JA: The complexity of NF-κB signaling in inflammation and cancer. Mol Cancer 12: 86, 2013.
67. Rasmi RR, Sakthivel KM and Guruvayoorappan C: NF-κB inhibitors in treatment and prevention of lung cancer. Biomed Pharmacother 130: 110569, 2020.
68. Sarkar FH and Li Y: NF-kappaB: A potential target for cancer chemoprevention and therapy. Front Biosci 13: 2950-2959, 2008.
69. Fouani L, Kovacevic Z and Richardson DR: Targeting oncogenic nuclear factor Kappa B Signaling with redox-active agents for cancer treatment. Antioxid Redox Signal 30: 1096-1123, 2019.
70. Suhail M, Tarique M, Muhammad N, Naz H, Hafeez A, Zughaibi TA, Kamal MA and Rehan M: A critical transcription factor NF-κB as a cancer therapeutic target and its inhibitors as cancer treatment options. Curr Med Chem 28: 4117-4132, 2021.
71. Khan H, Ullah H, Castilho P, Gomila AS, D'Onofrio G, Filosa R, Wang F, Nabavi SM, Daglia M, Silva AS, *et al*: Targeting NF-κB signaling pathway in cancer by dietary polyphenols. Crit Rev Food Sci Nutr 60: 2790-2800, 2020.
72. Rajagopal C, Lankadasari MB, Aranjani JM and Harikumar KB: Targeting oncogenic transcription factors by polyphenols: A novel approach for cancer therapy. Pharmacol Res 130: 273-291, 2018.
73. Ashrafizadeh M, Najafi M, Makvandi P, Zarrabi A, Farkhondeh T and Samarghandian S: Versatile role of curcumin and its derivatives in lung cancer therapy. J Cell Physiol 235: 9241-9268, 2020.
74. Saijo T, Ishii G, Ochiai A, Yoh K, Goto K, Nagai K, Kato H, Nishiwaki Y and Saijo N: Eg5 expression is closely correlated with the response of advanced non-small cell lung cancer to antimitotic agents combined with platinum chemotherapy. Lung Cancer 54: 217-225, 2006.
75. Lv P, Man S, Xie L, Ma L and Gao W: Pathogenesis and therapeutic strategy in platinum resistance lung cancer. Biochim Biophys Acta Rev Cancer 1876: 188577, 2021.
76. Wang LH, Li Y, Yang SN, Wang FY, Hou Y, Cui W, Chen K, Cao Q, Wang S, Zhang TY, *et al*: Gambogic acid synergistically potentiates cisplatin-induced apoptosis in non-small-cell lung cancer through suppressing NF-κB and MAPK/HO-1 signalling. Br J Cancer 110: 341-352, 2014.
77. Wang J, Tian L, Khan MN, Zhang L, Chen Q, Zhao Y, Yan Q, Fu L and Liu J: Ginsenoside Rg3 sensitizes hypoxic lung cancer cells to cisplatin via blocking of NF-κB mediated epithelial-mesenchymal transition and stemness. Cancer Lett 415: 73-85, 2018.
78. Cui H, Arnst K, Miller DD and Li W: Recent advances in elucidating paclitaxel resistance mechanisms in non-small cell lung cancer and strategies to overcome drug resistance. Curr Med Chem 27: 6573-6595, 2020.
79. Jiang N, Dong XP, Zhang SL, You QY, Jiang XT and Zhao XG: Triptolide reverses the Taxol resistance of lung adenocarcinoma by inhibiting the NF-κB signaling pathway and the expression of NF-κB-regulated drug-resistant genes. Mol Med Rep 13: 153-159, 2016.
80. Li DD, Qin XC, Yang Y, Chu HX, Li RL, Ma LX, Ding HW and Zhao QC: Daurinoline suppressed the migration and invasion of chemo-resistant human non-small cell lung cancer cells by reversing EMT and Notch-1 and sensitized the cells to Taxol. Environ Toxicol Pharmacol 66: 109-115, 2019.
81. Li Y ans Zhang H: Nanoparticle-based drug delivery systems for enhanced tumor-targeting treatment. J Biomed Nanotechnol 15: 1-27, 2019.